

Reflections of topological properties in the planar-Hall response for semimetals carrying pseudospin-1 quantum numbers

Firdous Haidar and Ipsita Mandal*

*Department of Physics, Shiv Nadar Institution of Eminence (SNIOE),
Gautam Buddha Nagar, Uttar Pradesh 201314, India*

We continue our investigations of the nature of the linear-response tensors in planar-Hall and planar-thermal Hall configurations, involving three-dimensional nodal-point semimetals, by considering here nodes hosting pseudospin-1 quasiparticles. Such systems exemplify multifold semimetals, as they have three bands crossing at a nodal point. We derive the explicit expressions of the electric, thermoelectric, and thermal coefficients, when the nodes are subjected to the combined influence of an electric field (and/or temperature gradient) and a weak (i.e., nonquantizing) magnetic field. In order to have a complete description, we consider the effects of the Berry curvature and the orbital magnetic moment on an equal footing, both of which originate from the underlying topological features of the bandstructure. Going beyond our previous works, we determine the out-of-plane response comprising the intrinsic anomalous-Hall and the Lorentz-force-contributed currents, and chalk out the effects of internode scatterings as well. Our theoretical explorations shed light on the mechanisms of transport in multifold semimetals, which are being investigated in contemporary experiments.

CONTENTS

I. Introduction	2
II. Model	3
A. Relevant topological quantities	4
B. Expansion in B	5
C. Linear-response coefficients	6
III. Magnetoelectric conductivity	7
A. Longitudinal component of $\bar{\sigma}_\chi$	7
B. In-plane transverse component of $\bar{\sigma}_\chi$	8
C. Out-of-plane component due to the anomalous-Hall effect	8
D. Part of the conductivity arising from the Lorentz-force operator	9
1. Comparison with WSMS/mWSMS	10
2. Comparison with RSW semimetals	10
IV. Magnetothermoelectric conductivity and magnetothermal coefficient	11
A. Longitudinal components	11
B. In-plane transverse components	11
C. Mott relation and Wiedemann-Franz law	11
V. Effects of internode scatterings	12
VI. Summary, discussions, and future perspectives	13
Acknowledgments	14
A. Identities for some useful integrals	14
B. Current from the Lorentz-force part	14
1. $n = 1$: Terms originating from the linear action of the Lorentz-force operator	15
2. $n = 2$: Terms originating from the quadratic action of the Lorentz-force operator	16
3. $n = 3$: Terms originating from the cubic action of the Lorentz-force operator	16
References	16

* ipsita.mandal@snu.edu.in

I. INTRODUCTION

There has been an immense amount of interest, comprising both theoretical and experimental efforts, for discovering and understanding novel transport characteristics shown by three-dimensional (3d) semimetals with symmetry-protected band-crossings. Such interest is triggered by the fact that, when a nodal point lies close to the Fermi level, the exotic signatures of transport-properties (such as the linear-response coefficients) often offer a glimpse of the mathematical concepts of topology being realized in the 3d Brillouin zone (BZ) of solid-state systems [1–8]. Due to the fact that the density-of-states vanishes identically at the nodal points, the semimetallic bands differ in their behaviour from both the insulators (characterized by a finite gap between the bands) and the conventional metals (characterized by an overlap in finite regions of the BZ and, thus, featuring a finite density-of-states). The usual semi-empirical approach of deriving the so-called $\mathbf{k} \cdot \mathbf{p}$ Hamiltonian, for visualizing the associated bandstructure, furnishes the low-energy effective Hamiltonian in the vicinity of a band-crossing point. For the case when we have $(2\zeta + 1)$ bands crossing at the point, in the 3d momentum space parametrized by $\mathbf{k} = \{k_x, k_y, k_z\}$, the Hamiltonian takes the form of $\mathbf{d}(\mathbf{k}) \cdot \mathbf{S}$, where $\mathbf{d}(\mathbf{k}) = \{d_x(\mathbf{k}), d_y(\mathbf{k}), d_z(\mathbf{k})\}$. Here, \mathbf{S} is the vector operator comprising the components $\{S_x, S_y, S_z\}$, representing the three components of the angular momentum operator in the spin- ζ representation of the SU(2) group. Therefore, an appropriate set of three $(2\zeta + 1) \times (2\zeta + 1)$ square matrices constitute a bonafide representation, reproducing the $(2\zeta + 1)$ -band system, with the bands carrying the azimuthal quantum numbers spanning from $-\zeta$ to ζ . Consequently, the energy levels are labelled with these *pseudospin* quantum numbers, invoking their analogy with the relativistic *spin* quantum numbers. While the latter set arises from the spatial rotations of the Lorentz group, representing the fundamental spacetime symmetries, the former set is the consequence of (nonrelativistic) crystal symmetries. One intriguing outcome is that integer-valued pseudospin quantum numbers are possible, corresponding to an odd number of fermionic bands crossing at a nodal point, in contrast with the fact that integer values of spin are forbidden for relativistic fermionic particles (as embodied in the spin-statistics theorem).

The poster-child of 3d semimetals is the pseudospin-1/2 Weyl semimetal (WSM) [1, 2, 9], featuring the simplest case of twofold band-crossing points, with a linear-in-momentum dispersion. Making things more exciting, multifold band-crossings have been discovered in the 65 chiral space groups comprising chiral crystals [6], which have only orientation-preserving symmetries. Such examples include pseudospin-1 triple-point semimetal (TSM) [4, 6, 8, 10–16] and pseudospin-3/2 Rarita-Schwinger-Weyl (RSW) semimetal [4, 6, 8, 10, 13–15, 17–26], which have three and four bands crossing at the nodal point, respectively.

The intensive interest in studying nodal-point semimetals primarily stems from the fact that their BZ harbours a nontrivial topology, with the nodes being the singular points of the vector-field lines of the Berry curvature (BC). The BC arises from the Berry phase, which endows the BZ with a nontrivial topology [3, 8, 25–34] (when we visualize the BZ as a closed 3d manifold). The Berry phase also gives rise to the orbital magnetic moment (OMM) as another intrinsic topological property. Such topological features manifest themselves in various transport measurements, e.g., intrinsic anomalous-Hall effect [35–37], nonzero planar-Hall response [3, 8, 25, 26, 29, 30, 32–34, 38–51], magneto-optical conductivity under quantizing magnetic fields [52–54], Magnus Hall effect [22, 55, 56], circular dichroism [13, 57], circular photogalvanic effect [58–61], and transmission of quasiparticles across potential barriers/wells [23, 62–64].

The nontriviality of topology is manifested by nonzero BC monopoles [65, 66], sitting at the nodal points, serving as topological charges, and sourcing the BC flux. These are equivalent to the Chern numbers, using the terminology from topology. The sign of the BC-monopole’s charge is demarcated as the chirality χ of the node, leading to the notion of *chiral* quasiparticles. They are said to be *right-handed* or *left-handed*, depending on whether $\chi = 1$ or $\chi = -1$. Summing over of all the topological charges in the BZ, carried either by the conduction or the valence bands of all the chirally-charged nodes, must give zero in a system resulting from electrons hopping on a crystal lattice. This is explained mathematically by the Nielsen-Ninomiya theorem [67]. In bandstructures, this is reflected by the fact that we must have conjugate pairs of nodes in the BZ, having $\chi = \pm 1$. The conventional way is to assign χ the sign of the monopole-charges of the negative-energy bands, where positive or negative is measured with respect to the band-touching point (assigned the zero of energy). Also, according to this convention, a positive (negative) sign is associated with a node taken to act as a source (sink) for BC-flux lines.

In this paper, we focus on 3d TSMs, carrying the pseudospin value of $\zeta = 1$, whose effective low-energy continuum Hamiltonian is of the form of $\mathbf{d}(\mathbf{k}) \cdot \mathbf{S}$ [cf. Fig. 1(a)]. Here, \mathbf{S} represents the vector of the three matrices forming a spin-1 representation of the SO(3) group. The pseudospin-1 quasiparticles can be realized in various systems and have been studied extensively in wide contexts [10, 12, 13, 16, 46, 68–81]. They are often dubbed as “Maxwell fermions” [70], reflecting the analogy with the spin-1 quantum number of the photons (which are described by the Maxwell equations).

When the effective low-energy dispersion of the quasiparticles, in the vicinity of a node, goes as $\sim \sqrt{\alpha_J^2 k_\perp^{2J} + v_z^2 k_z^2}$ (where $J \in \{1, 2, 3\}$, α_J is a material-dependent parameter, and $k_\perp = \sqrt{k_x^2 + k_y^2}$), it hosts a Chern number of magnitude $2J$ [12, 46, 81]. Therefore, for $J > 1$, they form the analogues of the pseudospin-1/2 multi-Weyl semimetals (mWSMs) [4, 30, 32–34, 82], differing in the number of bands and the value of the Chern number/monopole-charge (by a factor of two).

Here, we continue our explorations of planar-Hall and planar-thermal-Hall set-ups, comprising a semimetal subjected to the combined influence of an electric field, \mathbf{E} , (and/or a temperature gradient, $\nabla_r T$) and a magnetic field, \mathbf{B} , as depicted

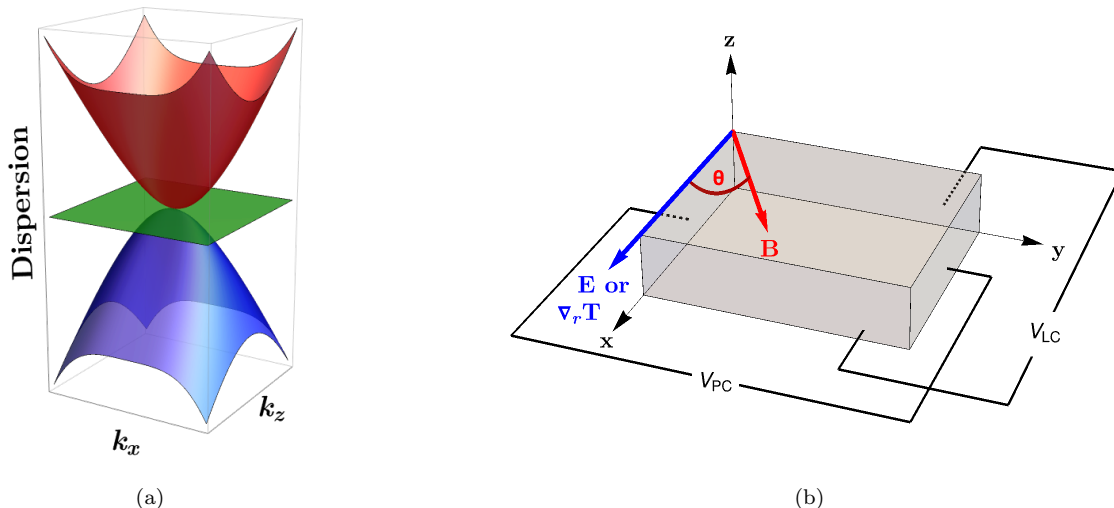


FIG. 1. (a) The dispersion of a single pseudospin-1 node, with $J = 2$, against the $k_z k_x$ -plane. (b) Schematics of the planar-Hall set-up where a semimetallic material, hosting pseudospin-1 quasiparticles, is probed with a static electric field $\mathbf{E} = E \hat{\mathbf{x}}$ (and/or temperature gradient $\nabla_r T = \partial_x T \hat{\mathbf{x}}$), under the action of a nonquantizing magnetic field \mathbf{B} . The latter makes an angle θ with respect to the electric field (and/or the temperature gradient). The in-plane voltages, generated parallel and perpendicular to $E \hat{\mathbf{x}}$ (or $\partial_x T \hat{\mathbf{x}}$), are indicated by V_{LC} and V_{PC} , respectively. The subscripts indicate their association with the longitudinal and transverse (i.e., planar-Hall) components of the resulting currents.

in Fig. 1(b). As pointed out above, we will consider the case when the semimetal harbours pseudospin-1 quasiparticles. In recent times, there have been extensive amounts of theoretical and experimental investigations involving the associated response coefficients [3, 8, 29, 30, 32–34, 38–50, 83, 84]. The plane containing \mathbf{E} (or $\nabla_r T$) and \mathbf{B} is chosen to be the xy -plane, with \mathbf{E} (or $\nabla_r T$) fixed along the x -axis. The direction of the magnetic field, $\mathbf{B} \equiv B(\cos\theta \hat{\mathbf{x}} + \sin\theta \hat{\mathbf{y}})$ (where $B \equiv |\mathbf{B}|$), is specified by the angle θ . Clearly, θ is the angle it makes with $\hat{\mathbf{x}}$, and is not necessarily equal to $\pi/2$ or $3\pi/2$ in general. We focus on the linear-response regimes with respect to the probe fields of \mathbf{E} and $\nabla_r T$. The relevant response tensors are the ones relating the electric and thermal currents to \mathbf{E} and $\nabla_r T$, which encompass the magnetoelectric conductivity (σ_χ), the magnetothermoelectric conductivity (α_χ), and the magnetothermal conductivity (κ_χ). Let ℓ_χ denote the tensor relating the heat current to the temperature gradient at a vanishing electric field. Knowing ℓ_χ , one can compute κ_χ — hence, ℓ_χ itself is often loosely referred to as the magnetothermal coefficient. In summary, if we know the three independent tensors embodied by σ_χ , α_χ , and ℓ_χ , we can construct all the response characteristics in transport measurements. It is worth mentioning that the nature of σ_χ and ℓ_χ has been studied in Ref. [46] for the case of $J = 2$, but without taking the OMM-induced contributions into account.

The paper is organized as follows: In Sec. II, we describe the explicit form of the low-energy effective Hamiltonian in the vicinity of a TSM node, for the three possible values of J . The resulting expressions for the BC and the OMM are also shown. Secs. III and IV are devoted to demonstrating the explicit expressions for the longitudinal and transverse components of σ_χ , α_χ , and ℓ_χ , respectively. In Sec. V, we discuss the effects of internode scatterings. Finally, we conclude with a summary and outlook in Sec. VI. The appendices are devoted to elaborating on much of the details of the intermediate steps, necessary to derive the final expressions shown in the main text. In all our expressions, we will be using the natural units, which means that the reduced Planck's constant (\hbar), the speed of light (c), and the Boltzmann constant (k_B) are each set to unity. Additionally, electric charge has no units, with the magnitude of a single electronic charge measuring $e = 1$.

II. MODEL

For the TSMs, which are characterized by nodal points with threefold degeneracies, we encounter two distinct situations that may arise to satisfy the Nielsen-Ninomiya theorem: Existence of a pair of conjugate nodes (1) of the same pseudospin variety, with $\chi = \pm 1$; (2) comprising bands of different pseudospin quantum numbers. The first case is exemplified by a pair of TSMS [4, 11]. The second possibility is exemplified by the following two cases:

(a) A single node of TSM is pinned at the centre of the BZ (i.e., the Γ -point), carrying a monopole charge of $+2$, while a fourfold-degenerate node (comprising two copies of WSMs of the same chirality) exists at the boundary of the BZ (i.e., the R -point) with a net monopole charge equalling $-1 - 1 = -2$. Candidate materials include CoSi [8].

(b) In a typical material harbouring an RSW node [14, 15, 85, 86], we find that there is the RSW node at the Γ -point

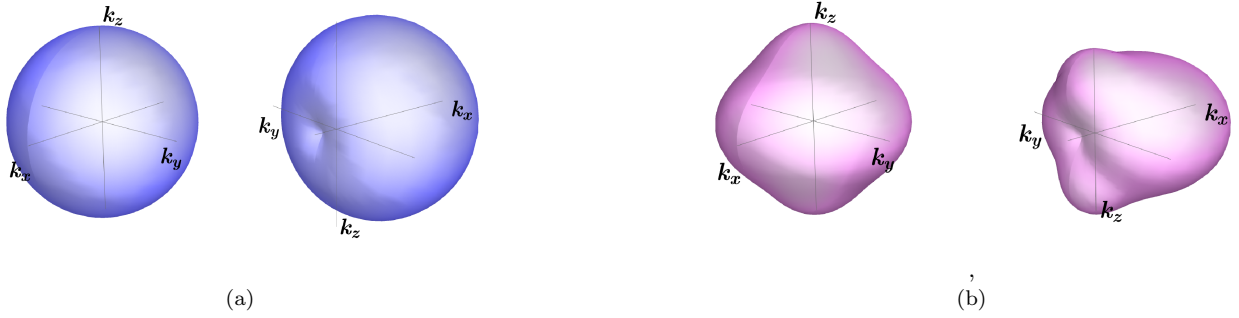


FIG. 2. Schematics of the Fermi surfaces for one node of a TSM with (a) $J=1$ and (b) $J=2$: In each subfigure, the two surfaces represent the case without and with the OMM-correction, respectively. Here, we have taken the applied magnetic field to be directed purely along the x -axis.

carrying $+4$ charge, and a sixfold-degenerate (originating from the doubling of pseudospin-1 excitations) at the R -point carrying -4 charge. Candidate materials include the SrGePt family (e.g., SrSiPd, BaSiPd, CaSiPt, SrSiPt, BaSiPt, and BaGePt) [15].

Expanding the $\mathbf{k} \cdot \mathbf{p}$ Hamiltonian about a threefold-degeneracy point in small $\{k_x, k_y, k_z\}$, we obtain the low-energy effective continuum Hamiltonian, embodied by [12, 46, 81]

$$\mathcal{H}_\chi(\mathbf{k}) = \mathbf{d}(\mathbf{k}) \cdot \mathbf{S}, \quad \mathbf{d}(\mathbf{k}) = \{\alpha_J k_\perp^J \cos(J\phi_k), \alpha_J k_\perp^J \sin(J\phi_k), \chi v_z k_z\}, \quad J \in \{1, 2, 3\},$$

$$k_\perp = \sqrt{k_x^2 + k_y^2}, \quad \phi_k = \arctan\left(\frac{k_y}{k_x}\right), \quad \alpha_J = \frac{v_\perp}{k_0^{J-1}}. \quad (1)$$

Here, $\mathbf{S} = \{S_x, S_y, S_z\}$ represents the vector operator of the pseudospin-1 representation of the $SO(3)$ group, $\chi \in \{1, -1\}$ denotes the chirality of the node, and v_z (v_\perp) is the Fermi velocity along the z -direction (xy -plane). The material-dependent parameter k_0 , with the dimension of momentum, will have its value determined by the microscopic details of the material under consideration. We note that the conventional $J = 1$ TSM is isotropic (forming an analogue of the isotropic WSMs), which is obtained by setting $v_\perp = v_z$. For calculational purposes, we choose the representation where

$$S_x = \frac{1}{\sqrt{2}} \begin{pmatrix} 0 & 1 & 0 \\ 1 & 0 & 1 \\ 0 & 1 & 0 \end{pmatrix}, \quad S_y = \frac{1}{\sqrt{2}} \begin{pmatrix} 0 & -i & 0 \\ i & 0 & -i \\ 0 & i & 0 \end{pmatrix}, \quad S_z = \begin{pmatrix} 1 & 0 & 0 \\ 0 & 0 & 0 \\ 0 & 0 & -1 \end{pmatrix}. \quad (2)$$

The energy eigenvalues of the Hamiltonian are given by

$$\varepsilon_s(\mathbf{k}) = s \epsilon_{\mathbf{k}}, \quad s \in \{-1, 0, 1\}, \quad \epsilon_{\mathbf{k}} = \sqrt{\alpha_J^2 k_\perp^{2J} + v_z^2 k_z^2}, \quad (3)$$

where the value $+1$ (-1) for s represents the conduction (valence) band. The value zero represents a nondispersive flat-band. An orthogonal set of eigenvectors can be represented as follows:

$$\left\{ -1, \frac{\chi \sqrt{2} k_z v_z e^{iJ\phi_k}}{\alpha_J k_\perp^J}, e^{2iJ\phi_k} \right\} \text{ for } s = 0 \text{ and}$$

$$\left\{ 1 + \frac{2\chi k_z v_z (\chi k_z v_z + s \epsilon_{\mathbf{k}})}{\alpha_J^2 k_\perp^{2J}}, \frac{\sqrt{2} e^{iJ\phi_k} (\chi k_z v_z + s \epsilon_{\mathbf{k}})}{\alpha_J k_\perp^J}, e^{2iJ\phi_k} \right\} \text{ for } s = \pm 1. \quad (4)$$

Clearly, for the two dispersive bands, the energy varies (1) linearly along the k_z -direction, and (2) as k_\perp^J when we confine to the $k_x k_y$ -plane [cf. Fig. 1(a)]. The group-velocity of the chiral quasiparticles, occupying the band with index s , is given by

$$\mathbf{v}_s(\mathbf{k}) \equiv \nabla_{\mathbf{k}} \varepsilon_s(\mathbf{k}) = \frac{s}{\epsilon_{\mathbf{k}}} \{ J \alpha_J^2 k_\perp^{2J-2} k_x, J \alpha_J^2 k_\perp^{2J-2} k_y, v_z^2 k_z \}. \quad (5)$$

A. Relevant topological quantities

We discuss here the vectors given by the Berry curvature (BC) and the orbital magnetic moment (OMM), which will affect the linear response that we are set out to compute. For the band with index s , these are expressed by the generic

formulae of [27, 87]

$$\boldsymbol{\Omega}_\chi^s(\mathbf{k}) = i \langle \nabla_{\mathbf{k}} \psi_\chi^s(\mathbf{k}) | \times | \nabla_{\mathbf{k}} \psi_\chi^s(\mathbf{k}) \rangle \text{ and } \mathbf{m}_\chi^s(\mathbf{k}) = \frac{-ie}{2} \langle \nabla_{\mathbf{k}} \psi_\chi^s(\mathbf{k}) | \times [\{ \mathcal{H}_\chi(\mathbf{k}) - \varepsilon_s(\mathbf{k}) \} | \nabla_{\mathbf{k}} \psi_\chi^s(\mathbf{k}) \rangle], \quad (6)$$

respectively. Here, $\{ | \psi_\chi^s(\mathbf{k}) \rangle \}$ is the set of normalized eigenvectors for the parent Hamiltonian.¹ On evaluating the expressions in Eq. (6) using $\mathcal{H}_\chi(\mathbf{k})$, we get

$$\begin{aligned} \boldsymbol{\Omega}_\chi^s(\mathbf{k}) &= \frac{-\chi s J v_z \alpha_J^2 k_\perp^{2J-2}}{\epsilon_{\mathbf{k}}^3} \{ k_x, k_y, J k_z \}, \\ \mathbf{m}_\chi^s(\mathbf{k}) &= \frac{-\chi e J v_z \mathcal{G}_s \alpha_J^2 k_\perp^{2J-2}}{2 \epsilon_{\mathbf{k}}^2} \{ k_x, k_y, J k_z \}, \text{ where } \mathcal{G}_s = \begin{cases} 1 & \text{for } s = \pm 1 \\ 2 & \text{for } s = 0 \end{cases}. \end{aligned} \quad (7)$$

For the flat-band, although the BC is identically zero, the OMM is nonzero and turns out to be twice the OMM of either of the dispersive bands. It is easy to verify from the $\boldsymbol{\Omega}_\chi^s(\mathbf{k})$ -expressions that the node has a net Chern number of $2\chi J$.

Due to the zero dispersion and zero BC for the flat-band, it leads to zero conductivity when OMM is ignored. Henceforth, we will then neglect the flat-band, as far as our calculations of linear response are concerned. We note that, for the dispersive bands, while the BC changes sign with s , the OMM does not. Therefore, for uncluttering of notations, we will henceforth remove the superscript ‘‘s’’ from $\mathbf{m}_\chi^s(\mathbf{k})$.

The first and foremost effect of BC is that it modifies the phase-space volume element via a factor of $[\mathcal{D}_\chi^s(\mathbf{k})]^{-1}$, where

$$\mathcal{D}_\chi^s(\mathbf{k}) = [1 + e \{ \mathbf{B} \cdot \boldsymbol{\Omega}_\chi^s(\mathbf{k}) \}]^{-1}. \quad (8)$$

A nonzero OMM causes a Zeeman-like correction to be added to the dispersion [27], leading to the effective dispersion of

$$\xi_\chi^s(\mathbf{k}) = \varepsilon_s(\mathbf{k}) + \varepsilon_\chi^{(m)}(\mathbf{k}), \quad \varepsilon_\chi^{(m)}(\mathbf{k}) = -\mathbf{B} \cdot \mathbf{m}_\chi(\mathbf{k}). \quad (9)$$

This, in turn, modifies the group-velocity as

$$\mathbf{w}_\chi^s(\mathbf{k}) \equiv \nabla_{\mathbf{k}} \xi_\chi^s(\mathbf{k}) = \mathbf{v}_s(\mathbf{k}) + \mathbf{u}_\chi^{(m)}(\mathbf{k}), \quad \mathbf{u}_\chi^{(m)}(\mathbf{k}) = \nabla_{\mathbf{k}} \varepsilon_\chi^{(m)}(\mathbf{k}). \quad (10)$$

The modified effective Fermi surface, on including the OMM-correction, is illustrated schematically in Fig. 2.

The effects of OMM will be show up in the equilibrium Fermi-Dirac distribution,

$$f_0(\xi_s^X(\mathbf{k}), \mu, T(\mathbf{r})) = \frac{1}{1 + \exp[(\xi_s^X(\mathbf{k}) - \mu) \beta(\mathbf{r})]}, \quad (11)$$

where $\beta(\mathbf{r}) = 1/T(\mathbf{r})$. While using f_0 in various equations, we will be suppressing its μ - and T -dependence for uncluttering of notations.

B. Expansion in B

In order to obtain closed-form analytical expressions, we will expand the B -dependent terms upto a given order in B , assuming it has a small magnitude. This is anyway an essential condition in order to neglect the quantization of the dispersion into discrete Landau levels, and for applying the semiclassical Boltzmann formalism using the effective dispersion of Eq. (9). More specifically, we must have a small cyclotron frequency, $\omega_c = eB/m^*$ (where m^* is the effective mass with the magnitude $\sim 0.11 m_e$ [88], with m_e denoting the electron mass). The regime of validity of our calculational framework holds when $\omega_c \ll \mu$, where μ is the energy at which the chemical potential cuts a dispersing band.

The weak-magnetic-field limit implies that

$$e |\mathbf{B} \cdot \boldsymbol{\Omega}_\chi^s| \ll 1 \text{ and } \left| \varepsilon_\chi^{(m)}(\mathbf{k}) \right| \ll |\varepsilon_s|. \quad (12)$$

In what follows, we will calculate all the terms upto $\mathcal{O}(B^2)$. This implies that we use the following expansions:

$$\mathcal{D}_\chi^s = 1 - e (\mathbf{B} \cdot \boldsymbol{\Omega}_\chi^s) + e^2 (\mathbf{B} \cdot \boldsymbol{\Omega}_\chi^s)^2 + \mathcal{O}(B^3), \quad f_0(\xi_\chi^s) = f_0(\varepsilon_s) + \varepsilon_\chi^{(m)} f_0'(\varepsilon_s) + \frac{1}{2} (\varepsilon_\chi^{(m)})^2 f_0''(\varepsilon_s) + \mathcal{O}(B^3). \quad (13)$$

Here, the ‘‘prime’’ superscript denotes partial-differentiation with respect to the variable shown explicitly within the brackets [e.g., $f_0'(\varepsilon) \equiv \partial_\varepsilon f_0(\varepsilon)$].

¹ For example, the set shown in Eq. (4) can be used after normalization.

C. Linear-response coefficients

Derived through the semiclassical Boltzmann equations, we will investigate the transport properties in the linear-response regime, applicable for small values of the probe fields of \mathbf{E} and $\nabla_r T$. Our planar-Hall and planar-thermal-Hall configurations are shown in Fig. 1(b). In the following sections, we will compute the resulting three linear-response coefficients, $\sigma_\chi(s)$, $\alpha_\chi(s)$, and $\ell_\chi(s)$, whose physical significance can be understood from the discussions below Eq. (14). We will consider a positive chemical potential μ being applied to the node, such that the Fermi level cuts the positive-energy band. Since the steps to obtain the forms of linear-response coefficients have been extensively discussed in Refs. [3, 25, 30], we do not review it here. We just use the final answers, which are explained below.

The linear-response coefficients relate the average electric and thermal current densities, \mathbf{J}_χ^s and $\mathbf{J}_\chi^{s,\text{th}}$, contributed by fermionic quasiparticles associated with the band s and node with chirality χ , to the driving electric potential gradient and temperature gradient. This relation is expressed in a compact form as [89]

$$\begin{bmatrix} (J_\chi^s)_i \\ (J_\chi^{s,\text{th}})_i \end{bmatrix} = \sum_j \begin{bmatrix} (\sigma_\chi)_{ij}(s) & (\alpha_\chi)_{ij}(s) \\ T(\alpha_\chi)_{ij}(s) & (\ell_\chi)_{ij}(s) \end{bmatrix} \begin{bmatrix} E_j \\ -\partial_j T \end{bmatrix}, \quad (14)$$

where $\{i, j\} \in \{x, y, z\}$ indicates the Cartesian components of the current vectors and the response tensors in 3d. While $\sigma_\chi(s)$ and $\alpha_\chi(s)$ represent the magnetoelectric conductivity and the magnetothermoelectric conductivity, respectively, $\ell_\chi(s)$ represents the tensor relating the thermal current density to the temperature gradient, at a vanishing electric field. Since it is used to compute the magnetothermal coefficient [3, 7, 25, 89], $\kappa_\chi(s)$, we will loosely refer to $\ell_\chi(s)$ itself as the magnetothermal coefficient.

In this subsection, we discuss the scenario when only the intranode scatterings play a dominant role, implemented through using a phenomenological momentum-independent relaxation time (τ). From the final expressions obtained from the *linearized* Boltzmann equations [25, 33], we divide up the electric conductivity into three parts as

$$\sigma_\chi(s) = \bar{\sigma}_\chi(s) + \sigma_\chi^{\text{AH}}(s) + \sigma_\chi^{\text{LF}}(s). \quad (15)$$

The contents and significance of these three parts are described below:

1. The first part arises from the current density of $\bar{\mathbf{J}}_\chi^s = -e^2 \tau \int \frac{d^3 \mathbf{k}}{(2\pi)^3} \mathcal{D}_\chi^s(\mathbf{w}_\chi^s + \mathbf{W}_\chi^s) (\mathbf{w}_\chi^s + \mathbf{W}_\chi^s) \cdot \mathbf{E} f'_0(\xi_\chi^s)$, and takes the form of

$$(\bar{\sigma}_\chi)_{ij}(s) = -e^2 \tau \int \frac{d^3 \mathbf{k}}{(2\pi)^3} \mathcal{D}_\chi^s [(w_\chi^s)_i + (W_\chi^s)_i] [(w_\chi^s)_j + (W_\chi^s)_j] f'_0(\xi_\chi^s), \quad \mathbf{W}_\chi^s = e (\mathbf{w}_\chi^s \cdot \boldsymbol{\Omega}_\chi^s) \mathbf{B}. \quad (16)$$

It comprises only even powers of B and has only nonzero in-plane components (i.e., the out-of-plane components vanish).

2. The second part comes from the electric current density of $\mathbf{J}_\chi^{s,\text{AH}} = -e^2 \int \frac{d^3 \mathbf{k}}{(2\pi)^3} (\mathbf{E} \times \boldsymbol{\Omega}_\chi^s) f_0(\xi_\chi^s)$, which gives rise to the ‘‘intrinsic anomalous-Hall effect’’ [35–37]. Hence,

$$(\sigma_\chi^{\text{AH}})_{ij}(s) = -e^2 \epsilon_{ijl} \int \frac{d^3 \mathbf{k}}{(2\pi)^3} (\Omega_\chi^s)^l f_0(\xi_\chi^s), \quad (17)$$

with its longitudinal component evaluating to zero (due to the presence of the Levi-Civita symbol). This part is completely independent of the relaxation time τ . If OMM is set to zero, $\sigma_\chi^{\text{AH}}(s)$ becomes independent of \mathbf{B} and, thus, vanishes identically. We also note that, for our set-up with the applied fields and temperature gradient confined to the xy -plane, the in-plane transverse component [i.e., $(\sigma_\chi^{\text{AH}})_{yx}(s)$] also vanishes, with only the out-of-plane transverse component surviving.

3. The third part is the so-called Lorentz-force part, and it arises from the current density of [25, 90]

$$\begin{aligned} \mathbf{J}_\chi^{s,\text{LF}} &= -e^2 \tau \int \frac{d^3 \mathbf{k}}{(2\pi)^3} (\mathbf{w}_\chi^s + \mathbf{W}_\chi^s) f'_0(\xi_\chi^s) \mathcal{Y}_\chi^s, \quad \text{where } \check{L} = (\mathbf{w}_\chi^s \times \mathbf{B}) \cdot \nabla_{\mathbf{k}} \\ \text{and } \mathcal{Y}_\chi^s &= \sum_{n=1}^{\infty} (e\tau \mathcal{D}_\chi^s)^n \check{L}^n [\mathcal{D}_\chi^s \{\mathbf{w}_\chi^s + \mathbf{W}_\chi^s\} \cdot \mathbf{E}]. \end{aligned} \quad (18)$$

This part arises from the action of the Lorentz-force operator, \check{L} , and the solution is obtained by expanding the summation series upto a certain value of n . The nomenclature reflects the fact that it includes the classical Hall effect due to the Lorentz force. The corresponding components of the electric conductivity is

$$(\sigma_\chi^{\text{LF}})_{ij}(s) = -e^2 \tau \int \frac{d^3 \mathbf{k}}{(2\pi)^3} [(w_\chi^s)_i + (W_\chi^s)_i] f'_0(\xi_\chi^s) \frac{\partial \mathcal{Y}_\chi^s}{\partial E_j}. \quad (19)$$

Regarding the magnetothermoelectric conductivity and the magnetothermal coefficient, we will only explicitly show the expressions for the in-plane components which arise from the non-anomalous-Hall and non-Lorentz-force parts (of the corresponding current densities). The relevant quantities are obtained from evaluating [25, 33]

$$(\bar{\alpha}_\chi)_{ij}(s) = e\tau \int \frac{d^3\mathbf{k}}{(2\pi)^3} \mathcal{D}_\chi^s [(w_\chi^s)_i + (W_\chi^s)_i] [(w_\chi^s)_j + (W_\chi^s)_j] \frac{(\xi_\chi^s - \mu)}{T} f'_0(\xi_\chi^s) \quad (20)$$

and

$$(\bar{\ell}_\chi)_{ij}(s) = -\tau \int \frac{d^3\mathbf{k}}{(2\pi)^3} \mathcal{D}_\chi^s \frac{(\xi_\chi^s - \mu)^2}{T} [(w_\chi^s)_i + (W_\chi^s)_i] [(w_\chi^s)_j + (W_\chi^s)_j] f'_0(\xi_\chi^s), \quad (21)$$

respectively.

In the following sections, we will demonstrate the explicit expressions for the three independent linear-response coefficients, viz. σ_χ , α_χ , and ℓ_χ . We assume a positive chemical potential μ being applied to the node in question, such that the Fermi level cuts the conduction band, which contributes to transport. Therefore, s is set equal to one and, henceforth, we will suppress the s -dependence.

III. MAGNETOELECTRIC CONDUCTIVITY

The generic expressions for the in-plane components of the magnetoelectric conductivity, obtained by expanding Eq. (16) (in powers of B) upto $\mathcal{O}(B^2)$, can be found in Ref. [33]. Here, we only show the final results applicable for TSMs. In fact, since the in-plane components contain only even powers of B , the expressions shown below are correct upto $\mathcal{O}(B^3)$. Notationwise, the superscript ‘‘Drude’’ refers to the B -independent parts. Furthermore, the superscripts of ‘‘BC’’ and ‘‘ m ’’ are used to indicate whether the OMM contributions have been set to zero or not. We also compute and demonstrate the expressions for the parts arising from the anomalous-Hall and Lorentz-force parts, which contain only odd powers of B , and are correct upto $\mathcal{O}(B^3)$. Hence, overall, all our expressions are correct upto $\mathcal{O}(B^3)$.

A. Longitudinal component of $\bar{\sigma}_\chi$

The part-by-part expressions for the longitudinal component of the electric conductivity are given by

$$\begin{aligned} (\sigma_\chi^{\text{Drude}})_{xx} &= \frac{e^2 \tau J}{6 \pi^2 v_z} \Upsilon_2(\mu, T), \quad (\sigma_\chi^{\text{BC}})_{xx} = \frac{e^4 \tau v_z \alpha_J^{\frac{2}{J}} \Upsilon_{-\frac{2}{J}}(\mu, T)}{128 \pi^{\frac{3}{2}}} \frac{\Gamma(\frac{2J-1}{J})}{\Gamma(\frac{9J-2}{2J})} [g_x^{bc}(J) B_x^2 + g_y^{bc}(J) B_y^2], \\ (\sigma_\chi^m)_{xx} &= \frac{e^4 \tau v_z \alpha_J^{\frac{2}{J}} \Upsilon_{-\frac{2}{J}}(\mu, T)}{128 \pi^{\frac{3}{2}}} \frac{\Gamma(\frac{2J-1}{J})}{\Gamma(\frac{9J-2}{2J})} [g_x^m(J) B_x^2 + g_y^m(J) B_y^2], \end{aligned} \quad (22)$$

where

$$\begin{aligned} g_x^{bc}(J) &= 4J(32J^2 - 19J + 3), \quad g_y^{bc}(J) = 4J(3J - 1)(2J - 1), \\ g_x^m(J) &= \frac{59J^4 - 175J^3 + 115J^2 - 27J + 2}{J}, \quad g_y^m(J) = \frac{J^4 - 25J^3 + 7J^2 + 7J - 2}{J}, \end{aligned} \quad (23)$$

and

$$\Upsilon_n(\mu, T) = \mu^n \left[1 + \frac{\pi^2 n(n-1)}{6} (T/\mu)^2 + \mathcal{O}\left((T/\mu)^3\right) \right] \text{ [arising from the Sommerfeld expansion shown in Eq. (A5)].} \quad (24)$$

Their behaviour is depicted in Fig. 3. In particular, we find that

$$\begin{aligned} \{g_x^{bc}(1), g_x^{bc}(2), g_x^{bc}(3)\} &= \{64, 744, 2808\}, \quad \{g_x^m(1), g_x^m(2), g_x^m(3)\} = \{-26, -24, 1010/3\}, \\ \{g_y^{bc}(1), g_y^{bc}(2), g_y^{bc}(3)\} &= \{8, 120, 480\}, \quad \{g_y^m(1), g_y^m(2), g_y^m(3)\} = \{-12, -72, -512/3\}. \end{aligned}$$

This leads to following conclusions:

- (1) $g_x^{bc}(J)$ and $g_y^{bc}(J)$ are positive for all J -values.
- (2) $g_x^m(J)$ is negative for $J = 1$ and $J = 2$, and positive for $J = 3$.
- (3) $g_y^m(J)$ is negative for all J -values.

Therefore, for $J = 1$ and $J = 2$, the OMM acts in opposition to the BC-only term for the B_x^2 -dependent part, thus

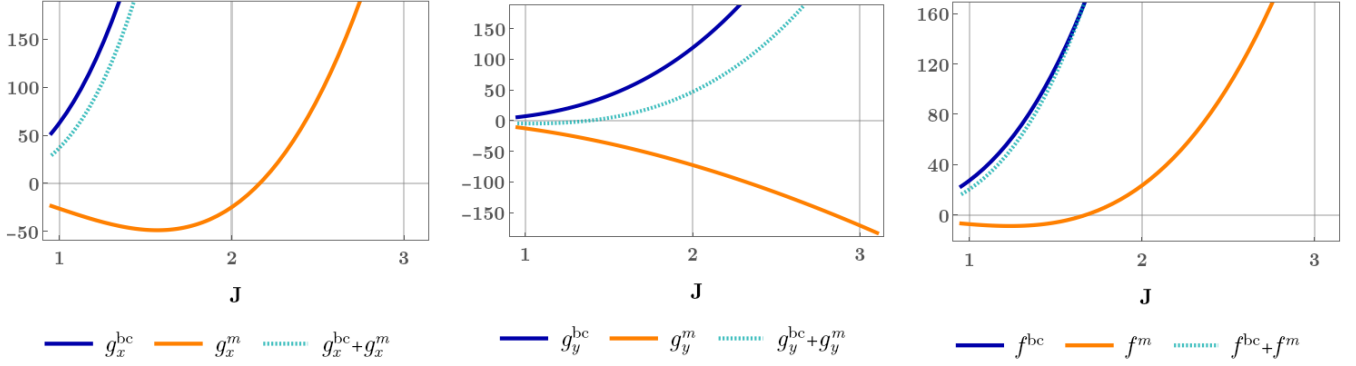


FIG. 3. Comparison of the values of the functions defined in Eqs. (23) and (26) for $J = 1, 2, 3$.

reducing the intensity of the overall response. On the other hand, for $J = 3$, the OMM-part adds up to the BC-only term, thus increasing the overall response for the B_x^2 -dependent part. However, for all values of J , the addition of the OMM does not change the sign of the overall response. Next, considering the B_y^2 -dependent part, we find that the BC-only and the OMM parts have opposite signs for all values of J . While the OMM-part manages to flip the sign of the overall response for $J = 1$, its magnitude is too low to do so for $J = 2$ and $J = 3$. All these values can be compared with the results for WSMs and mWSMs, shown in Ref. [33].

B. In-plane transverse component of $\bar{\sigma}_\chi$

The part-by-part expressions for the in-plane transverse component are given by

$$\begin{aligned}
 (\sigma_\chi^{\text{Drude}})_{yx} &= 0, & (\sigma_\chi^{\text{BC}})_{yx} &= \frac{e^4 \tau v_z \alpha_J^{\frac{2}{J}} \Upsilon_{-\frac{2}{J}}(\mu, T)}{64 \pi^{\frac{3}{2}}} \frac{\Gamma(\frac{2J-1}{J})}{\Gamma(\frac{9J-2}{2J})} f^{bc}(J) B_x B_y, \\
 (\sigma_\chi^m)_{yx} &= \frac{e^4 \tau v_z \alpha_J^{\frac{2}{J}} \Upsilon_{-\frac{2}{J}}(\mu, T)}{64 \pi^{\frac{3}{2}}} \frac{\Gamma(\frac{2J-1}{J})}{\Gamma(\frac{9J-2}{2J})} f^m(J) B_x B_y,
 \end{aligned} \tag{25}$$

where

$$f^{bc}(J) = 4J(13J^2 - 7J + 1), \quad f^m(J) = 29J^3 - 75J^2 + 54J - 17 + \frac{2}{J}. \tag{26}$$

Their behaviour is depicted in Fig. 3. In particular, we find that

$$\{f^{bc}(1), f^{bc}(2), f^{bc}(3)\} = \{28, 312, 1164\}, \quad \{f^m(1), f^m(2), f^m(3)\} = \{-7, 24, 761/3\}.$$

This leads to following conclusions: For $J = 1$, the BC-only and the OMM parts have opposite signs and, thus, the OMM-part reduces the magnitude of the overall response. For each of $J = 2$ and $J = 3$, the OMM-part adds up to the BC-only term, thus reinforcing each other. However, for all values of J , the addition of the OMM does not change the sign of the overall response. All these values can be compared with the results for WSMs and mWSMs, shown in Ref. [33].

C. Out-of-plane component due to the anomalous-Hall effect

For the intrinsic anomalous-Hall part, we actually need to expand $f_0(\xi_\chi^s)$ upto order B^3 , because it comprises only odd powers of B and we, ultimately, want to include the results for all components correct upto order B^3 (see the appendix of Ref. [25] for more details). Therefore, using

$$f_0(\xi_\chi^s) = f_0(\varepsilon_s) + \varepsilon_\chi^{(m)} f_0'(\varepsilon_s) + \frac{1}{2} (\varepsilon_\chi^{(m)})^2 f_0''(\varepsilon_s) + \frac{1}{6} (\varepsilon_\chi^{(m)})^3 f_0'''(\varepsilon_s) + \mathcal{O}(B^4),$$

the application of the Sommerfeld expansion [cf. Eq. (A5)] yields

$$(\sigma_\chi^{\text{AH}})_{zx} = \frac{-e^3 v_z J B_y}{2 \pi^2} \left[\frac{\Upsilon_{-1}(\mu, T)}{6} + \frac{B^2 e^2 v_z^2 \alpha_J^{\frac{2}{J}} \sqrt{\pi} \Gamma(\frac{4J-1}{J}) h_J}{128 \Gamma(\frac{9J-2}{2J})} \Upsilon_{-3J-2}(\mu, T) \right], \quad h_J = J(J+1)(J+2). \tag{27}$$

It does not have any BC-only contribution. Let us compare the above expression with the one for a single node of the WSM/mWSM variety. On carrying out explicit computations using the Hamiltonian shown in Ref. [33], we find it to be

$$(\sigma_\chi^{\text{AH}})_{zx} \Big|_{\text{mWSM}} = \frac{-e^3 v_z J B_y}{2\pi^2} \left[\frac{\Upsilon_{-1}(\mu, T)}{12} + \frac{B^2 e^2 v_z^2 \alpha_J^{\frac{2}{J}} \sqrt{\pi} \Gamma\left(\frac{4J-1}{J}\right) h_J}{256 \Gamma\left(\frac{9J-2}{2J}\right)} \Upsilon_{-\frac{3J-2}{J}}(\mu, T) \right]. \quad (28)$$

The analogous contribution for a single RSW node can be found in Ref. [25].

D. Part of the conductivity arising from the Lorentz-force operator

We divide up the part of the conductivity, σ_χ^{LF} , arising from the Lorentz-force operator [cf. Eq. (19)] into three subparts, which represent the contributions arising (1) independent of the topological properties like BC and OMM (this one includes the part giving rise to the conventional Hall effect); (2) purely from the BC (i.e., when OMM is neglected), and (3) when OMM is included:

$$\sigma_\chi^{\text{LF}} = \sigma_\chi^{\text{LF,H}} + \sigma_\chi^{\text{LF,BC}} + \sigma_\chi^{\text{LF,m}}. \quad (29)$$

Appendix B contains more details regarding the derivations of the generic expressions, expanded upto order B^3 . An important point to notice is that the Lorentz-force operator gives rise to in-plane components, in addition to the out-of-plane ones, which are evident only when we consider terms arising from $n \geq 2$ from the summation series shown in Eq. (18). Let us summarize our results below:

1. $n = 1$:

Using the generic expression shown in Appendix B1, we get nonzero values only for the out-of-plane parts. They take the forms of

$$\begin{aligned} (\sigma_\chi^{\text{LF,H}})_{zx} &= \frac{-e^3 v_z J \tau^2 B_y}{6\pi^2} \Upsilon_1(\mu, T), & (\sigma_\chi^{\text{LF,BC}})_{zx} &= \frac{-3 J^3 e^5 v_z^3 \tau^2 \alpha_J^{\frac{2}{J}} B_y B^2}{16\pi^{\frac{3}{2}}} \frac{\Gamma\left(\frac{3J-1}{J}\right)}{\Gamma\left(\frac{9J-2}{2J}\right)} \Upsilon_{-\frac{J+2}{J}}(\mu, T), \\ (\sigma_\chi^{\text{LF,m}})_{zx} &= \frac{e^5 v_z^3 \tau^2 \alpha_J^{\frac{2}{J}} B_y B^2}{128\pi^{\frac{3}{2}}} \frac{\Gamma\left(\frac{3J-1}{J}\right)}{\Gamma\left(\frac{9J-2}{2J}\right)} \mathcal{L}_J^m \Upsilon_{-\frac{J+2}{J}}(\mu, T), \text{ where } \mathcal{L}_J^m = 10 J^3 + 21 J^2 + J - 2. \end{aligned} \quad (30)$$

2. $n = 2$:

For the generic expression shown in Appendix B2, when we evaluate the integrals, we find that only in-plane components appear as the nonzero parts. They take the forms of

$$(\sigma_\chi^{\text{LF,BC}})_{xx} = (\sigma_\chi^{\text{LF,m}})_{xx} = 0, \quad (\sigma_\chi^{\text{LF,H}})_{xx} = \frac{-e^4 \tau^3 v_z \alpha_J^{\frac{2}{J}} \Upsilon_{\frac{2J-2}{J}}(\mu, T)}{16\pi^{\frac{3}{2}}} \frac{\Gamma\left(\frac{2J-1}{J}\right)}{\Gamma\left(\frac{7J-2}{2J}\right)} [n_x(J) B_x^2 + n_y(J) B_y^2],$$

$$\text{where } n_x(J) = J(J-1)^2, \quad n_y(J) = 3J^3 - 2J^2 + J; \quad (31)$$

and

$$(\sigma_\chi^{\text{LF,BC}})_{yx} = (\sigma_\chi^{\text{LF,m}})_{yx} = 0, \quad (\sigma_\chi^{\text{LF,H}})_{yx} = \frac{B_x B_y e^4 J^3 \tau^3 v_z \alpha_J^{\frac{2}{J}} \Upsilon_{\frac{2J-2}{J}}(\mu, T)}{8\pi^{\frac{3}{2}}} \frac{\Gamma\left(\frac{2J-1}{J}\right)}{\Gamma\left(\frac{7J-2}{2J}\right)}. \quad (32)$$

We observe that the in-plane components are generated exclusively from the BC- and OMM-independent contributions coming from Eq. (B12).

3. $n = 3$:

On evaluating the integrals using the generic expression shown in Appendix B3, we conclude that only the zx -component survives. It is given by

$$(\sigma_\chi^{\text{LF,H}})_{zx} = \frac{e^5 v_z^3 \tau^4 \alpha_J^{\frac{2}{J}} B_y B^2}{16\pi^{\frac{3}{2}}} \frac{\Gamma\left(\frac{2J-1}{J}\right)}{\Gamma\left(\frac{7J-2}{2J}\right)} (3J^3 - 2J^2 + J) \Upsilon_{\frac{J-2}{J}}(\mu, T). \quad (33)$$

Similar to the terms under $n = 2$, the $n = 3$ term is generated exclusively from the BC- and OMM-independent contributions. In this case, they arise from Eq. (B15).

Our results show that only currents proportional to odd powers of B and even powers of τ survive for the out-of plane component. On the other hand, the in-plane components contain only even powers of B and odd powers of τ . Gathering all the contributions shown above, we get the total for the out-of-plane part as

$$(\sigma_{\chi}^{\text{LF}})_{zx} = \frac{-e^3 v_z J \tau^2 B_y}{2 \pi^2} \left[\frac{\Upsilon_1(\mu, T)}{3} + \frac{e^2 v_z^2 B^2 \alpha_J^{\frac{2}{J}} \sqrt{\pi}}{8} \left\{ \frac{\Gamma(\frac{3J-1}{J})}{8 \Gamma(\frac{9J-2}{2J})} \mathcal{L}_{J,1} \Upsilon_{-J+2}(\mu, T) - \frac{\tau^2 \Gamma(\frac{2J-1}{J})}{\Gamma(\frac{7J-2}{2J})} \mathcal{L}_{J,2} \Upsilon_{\frac{J-2}{J}}(\mu, T) \right\} \right],$$

$$\text{where } \mathcal{L}_{J,1} = 14 J^2 - 21 J - 1 + \frac{2}{J} \text{ and } \mathcal{L}_{J,2} = 3 J^2 - 2 J + 1. \quad (34)$$

1. Comparison with WSMs/mWSMs

Using the Hamiltonian shown in Ref. [33], we now compare TSMs' behaviour with the results we derive for the WSMs/mWSMs. For a conduction band, the individual terms arising from $n = 1, 2, 3$ are shown below:

1. $n = 1$:

$$\begin{aligned} (\sigma_{\chi}^{\text{LF,H}})_{zx} &= \frac{-e^3 v_z J \tau^2 B_y}{6 \pi^2} \Upsilon_1(\mu, T), & (\sigma_{\chi}^{\text{LF,BC}})_{zx} &= \frac{-3 J^3 e^5 v_z^3 \tau^2 \alpha_J^{\frac{2}{J}} B_y B^2}{64 \pi^{\frac{3}{2}}} \frac{\Gamma(\frac{3J-1}{J})}{\Gamma(\frac{9J-2}{2J})} \Upsilon_{-J+2}(\mu, T), \\ (\sigma_{\chi}^{\text{LF,m}})_{zx} &= \frac{e^5 v_z^3 \tau^2 \alpha_J^{\frac{2}{J}} B_y B^2}{128 \pi^{\frac{3}{2}}} \frac{\Gamma(\frac{2J-1}{J})}{\Gamma(\frac{9J-2}{2J})} \tilde{\mathcal{L}}_J^m \Upsilon_{-J+2}(\mu, T), \text{ where } \tilde{\mathcal{L}}_J^m = 7 J^3 + 13 J^2 + J - 9 + \frac{2}{J}. \end{aligned} \quad (35)$$

Here, only the out-of-plane component survives.

2. $n = 2$:

Here, only in-plane components are generated, which turn out to be the same as the expressions shown in Eqs. (31) and (32). This is no surprise because there is no nonzero BC- or OMM-contributed part. The two systems differ only through the value of BC (differing by a factor of two) for the dispersing bands.

3. $n = 3$:

It turns out to be the same as Eq. (33), again because there is no nonzero BC- or OMM-contributed part.

Gathering all the contributions shown above, the net zx -part evaluates to

$$(\sigma_{\chi}^{\text{LF}})_{zx} = \frac{-e^3 v_z J \tau^2 B_y}{2 \pi^2} \left[\frac{\Upsilon_1(\mu, T)}{3} + \frac{e^2 v_z^2 B^2 \alpha_J^{\frac{2}{J}} \sqrt{\pi}}{8} \left\{ \frac{\Gamma(\frac{2J-1}{J})}{8 \Gamma(\frac{9J-2}{2J})} \tilde{\mathcal{L}}_{J,1} \Upsilon_{-J+2}(\mu, T) - \frac{\tau^2 \Gamma(\frac{2J-1}{J})}{\Gamma(\frac{7J-2}{2J})} \tilde{\mathcal{L}}_{J,2} \Upsilon_{\frac{J-2}{J}}(\mu, T) \right\} \right],$$

$$\text{where } \tilde{\mathcal{L}}_{J,1} = 5 J^2 - 19 J - 1 + \frac{9}{J} - \frac{2}{J^2} \text{ and } \tilde{\mathcal{L}}_{J,2} = \mathcal{L}_{J,2}. \quad (36)$$

2. Comparison with RSW semimetals

Let us compare the $J = 1$ TSM case with an *RSW node* (with two valence and two conduction bands), both of which have an isotropic linear-in- k dispersion of the bands. Of course, the $J = 1$ TSM corresponds to $v_{\perp} = v_z$, due to isotropy. In Ref. [25], although we discussed the results for $n = 1$, the results for $n = 2$ and $n = 3$ were not computed. Due to the presence of two conduction bands for the case of the RSW node, we use the index \check{s} to label them, where $\check{s} \in \{\frac{1}{2}, \frac{3}{2}\}$. Collecting the results till $n = 3$ and upto order $\mathcal{O}(B^3)$, the $\mu > 0$ condition leads to

$$\begin{aligned} (\sigma_{\chi}^{\text{LF,BC}})_{xx}(\check{s}) &= (\sigma_{\chi}^{\text{LF,m}})_{xx}(\check{s}) = 0, & (\sigma_{\chi}^{\text{LF,H}})_{xx}(\check{s}) &= \frac{-e^4 \tau^3 \check{s}^3 v_z^3 \Upsilon_0(\mu, T)}{6 \pi^2} B_y^2, \\ (\sigma_{\chi}^{\text{LF,BC}})_{yx}(\check{s}) &= (\sigma_{\chi}^{\text{LF,m}})_{yx}(\check{s}) = 0, & (\sigma_{\chi}^{\text{LF,H}})_{yx}(\check{s}) &= \frac{e^4 \tau^3 \check{s}^3 v_z^3 \Upsilon_0(\mu, T)}{6 \pi^2} B_x B_y, \\ (\sigma_{\chi}^{\text{LF}})_{zx}(\check{s}) &= \frac{-e^3 \check{s} \tau^2 v_z B_y}{2 \pi^2} \left[\frac{\Upsilon_1(\mu, T)}{3} + \frac{e^2 \check{s}^2 v_z^4 B^2}{15} \{ (\check{\mathcal{G}}_{\check{s}}^2 - 8 \check{\mathcal{G}}_{\check{s}} \check{s}^2 + 3 \check{s}^4) \Upsilon_{-3}(\mu, T) - 5 \check{s}^2 \tau^2 \Upsilon_{-1}(\mu, T) \} \right], \end{aligned} \quad (37)$$

where $\{\check{\mathcal{G}}_{1/2}, \check{\mathcal{G}}_{3/2}\} = \{\frac{7}{4}, \frac{3}{4}\}$. The zx -component contains nonzero values of $(\sigma_{\chi}^{\text{LF,H}})_{zx}(\check{s})$, $(\sigma_{\chi}^{\text{LF,BC}})_{zx}(\check{s})$, and $(\sigma_{\chi}^{\text{LF,m}})_{zx}(\check{s})$.

IV. MAGNETOTHERMOELECTRIC CONDUCTIVITY AND MAGNETOTHERMAL COEFFICIENT

We divide up the expressions for $\bar{\alpha}_s^\chi$ and $\bar{\ell}_s^\chi$, shown in Eqs. (20) and (21), into three parts as

$$\bar{\alpha}_s^\chi = \alpha_s^{\chi,\text{Drude}} + \alpha_s^{\chi,\text{BC}} + \alpha_s^{\chi,m} \quad \text{and} \quad \bar{\ell}_s^\chi = \ell_s^{\chi,\text{Drude}} + \ell_s^{\chi,\text{BC}} + \ell_s^{\chi,m}. \quad (38)$$

Analogous to the case of $\bar{\sigma}_s^\chi$, (1) the first part stands for the Drude contribution; (2) the second part arises solely due to the effect of the BC and survives when OMM is set to zero; and (3) the third part is the one which goes to zero if OMM is ignored. The generic expressions, obtained by expanding Eqs. (20) and (21) (in powers of B), can be found in Ref. [33]. Here, we only show the final results applicable for TSMs. Needless to emphasize that, since these in-plane components contain only even powers of B , the expressions shown below are correct upto $\mathcal{O}(B^3)$.

A. Longitudinal components

The part-by-part expressions for the longitudinal components are given by

$$\begin{aligned} (\alpha_\chi^{\text{Drude}})_{xx} &= \frac{-e\tau J\mu T}{9v_z}, & (\alpha_\chi^{\text{BC}})_{xx} &= \frac{\sqrt{\pi}e^3\tau v_z\alpha_J^{\frac{2}{J}}T}{192\mu^{\frac{2+J}{J}}}\frac{\Gamma(\frac{2J-1}{J})}{\Gamma(\frac{9J-2}{2J})}\frac{g_x^{bc}(J)B_x^2 + g_y^{bc}(J)B_y^2}{J}, \\ (\alpha_\chi^m)_{xx} &= \frac{\sqrt{\pi}e^3\tau v_z\alpha_J^{\frac{2}{J}}T}{192\mu^{\frac{2+J}{J}}}\frac{\Gamma(\frac{2J-1}{J})}{\Gamma(\frac{9J-2}{2J})}\frac{g_x^m(J)B_x^2 + g_y^m(J)B_y^2}{J}, \end{aligned} \quad (39)$$

$$\begin{aligned} (\ell_\chi^{\text{Drude}})_{xx} &= \frac{J\tau\mu^2 T}{18v_z}, & (\ell_\chi^{\text{BC}})_{xx} &= \frac{\sqrt{\pi}e^2\tau v_z\alpha_J^{\frac{2}{J}}T}{384\mu^{\frac{2}{J}}}\frac{\Gamma(\frac{2J-1}{J})}{\Gamma(\frac{9J-2}{2J})}[g_x^{bc}(J)B_x^2 + g_y^{bc}(J)B_y^2], \\ (\ell_\chi^m)_{xx} &= \frac{\sqrt{\pi}e^2\tau v_z\alpha_J^{\frac{2}{J}}T}{384\mu^{\frac{2}{J}}}\frac{\Gamma(\frac{2J-1}{J})}{\Gamma(\frac{9J-2}{2J})}[g_x^m(J)B_x^2 + g_y^m(J)B_y^2]. \end{aligned} \quad (40)$$

B. In-plane transverse components

The part-by-part expressions for the in-plane transverse components are given by

$$\begin{aligned} (\alpha_\chi^{\text{Drude}})_{yx} &= 0, & (\alpha_\chi^{\text{BC}})_{yx} &= \frac{\sqrt{\pi}e^3\tau v_z\alpha_J^{\frac{2}{J}}T}{96\mu^{\frac{2+J}{J}}}\frac{\Gamma(\frac{2J-1}{J})}{\Gamma(\frac{9J-2}{2J})}\frac{f^{bc}(J)B_x B_y}{J}, \\ (\alpha_\chi^m)_{yx} &= \frac{\sqrt{\pi}e^3\tau v_z\alpha_J^{\frac{2}{J}}T}{96\mu^{\frac{2+J}{J}}}\frac{\Gamma(\frac{2J-1}{J})}{\Gamma(\frac{9J-2}{2J})}\frac{f^m(J)B_x B_y}{J}, \end{aligned} \quad (41)$$

$$\begin{aligned} (\ell_\chi^{\text{Drude}})_{yx} &= 0, & (\ell_\chi^{\text{BC}})_{yx} &= \frac{\sqrt{\pi}e^2\tau v_z\alpha_J^{\frac{2}{J}}T}{192\mu^{\frac{2}{J}}}\frac{\Gamma(\frac{2J-1}{J})}{\Gamma(\frac{9J-2}{2J})}f^{bc}(J)B_x B_y, \\ (\ell_\chi^m)_{yx} &= \frac{\sqrt{\pi}e^2\tau v_z\alpha_J^{\frac{2}{J}}T}{192\mu^{\frac{2}{J}}}\frac{\Gamma(\frac{2J-1}{J})}{\Gamma(\frac{9J-2}{2J})}f^m(J)B_x B_y. \end{aligned} \quad (42)$$

C. Mott relation and Wiedemann-Franz law

From the explicit expressions of the in-plane longitudinal and transverse components of $\bar{\sigma}_\chi$, $\bar{\alpha}_\chi$, and $\bar{\ell}_\chi$ [cf. Eqs. (22), (25), (39), (40),(41), and (42)], we can immediately verify that the relations,

$$\partial_\mu(\bar{\sigma}_\chi)_{ij} = -\frac{3e}{\pi^2 T}(\bar{\alpha}_\chi)_{ij} + \mathcal{O}(T^2) \quad \text{and} \quad (\bar{\sigma}_\chi)_{ij} = \frac{3e^2}{\pi^2 T}(\bar{\ell}_\chi)_{ij} + \mathcal{O}(T^2), \quad (43)$$

hold. These two are the Mott relation and the Wiedemann-Franz law, respectively, which relate the three response-tensors in the limit $\beta \rightarrow \infty$ [89]. In particular, their validity in the presence of BC and OMM confirms that the relations hold in generic situations [91]. Consequently, if we know the nature of the magnetoelectric conductivity, we can infer the nature of the remaining two coefficients by using the above equations.

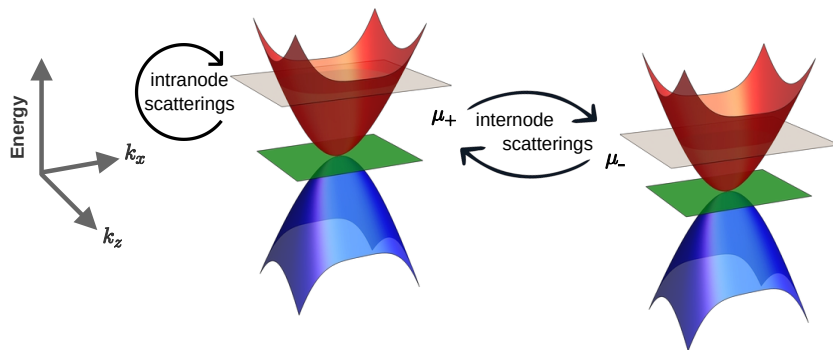


FIG. 4. Schematics of the scattering processes between two nodes of $J = 2$ TSM of opposite chiralities. The values of the chemical potential have been tuned to cut the positive-energy dispersive band at each node.

V. EFFECTS OF INTERNODE SCATTERINGS

Till now, we have focused only on intranode scatterings, ignoring any internode processes. This section will be dedicated to understanding how the internode scatterings affect the magnetoelectric-conductivity tensor, characterized by a phenomenological relaxation time, τ_G . We will not discuss the corresponding influence on the magnetothermoelectric and magnetothermal coefficients assuming that the Mott relation and the Wiedemann-Franz law will hold, and ensure that their nature can be determined from that of the magnetoelectric-conductivity tensor.

To start with, let us assume that initially, in the infinite past (denoted by time $t = -\infty$), both the nodes had the same chemical potential E_F , characterized by the distribution function $f_0(\varepsilon) = \left[1 + e^{\frac{\varepsilon - E_F}{T}}\right]^{-1}$, in the absence of any externally applied fields. Eventually, on applying the electromagnetic fields, there is the onset of the chiral anomaly [84, 92–96], causing the two conjugate nodes (with $\chi = \pm 1$) to acquire a local equilibrium value of the chemical potential, given by μ_χ . Therefore, the local equilibrium distribution function at each node is given by

$$f_{s,L}^\chi \simeq f_0(\xi_\chi^s) + [-f_0'(\xi_\chi^s)] \delta\mu_\chi, \quad \delta\mu_\chi \equiv \mu_\chi - E_F. \quad (44)$$

We define the average of an observable \mathcal{O} , at a node with chirality χ , as

$$\bar{\mathcal{O}}_\chi \equiv \langle \mathcal{O}_\chi^s(\xi_\chi^s(\mathbf{k}), E_F, T) \rangle = \frac{\sum_s \int \frac{d^3\mathbf{k}}{(2\pi)^3} (\mathcal{D}_\chi^s(\mathbf{k}))^{-1} [-f_0'(\xi_\chi^s(\mathbf{k}))] \mathcal{O}_\chi^s(\xi_\chi^s(\mathbf{k}), E_F, T)}{\sum_{\tilde{s}} \int \frac{d^3\mathbf{q}}{(2\pi)^3} (\mathcal{D}_\chi^{\tilde{s}}(\mathbf{q}))^{-1} [-f_0'(\xi_\chi^{\tilde{s}}(\mathbf{q}))]}, \quad (45)$$

where s and \tilde{s} are the band indices. Let us define

$$\mu_G = \frac{\mu_\chi + \mu_{-\chi}}{2}, \quad \rho_\chi \equiv \sum_s \int \frac{d^3\mathbf{k}}{(2\pi)^3} (\mathcal{D}_\chi^s(\mathbf{k}))^{-1} [-f_0'(\xi_\chi^s(\mathbf{k}))], \quad \rho_G = \frac{\rho_\chi + \rho_{-\chi}}{2}. \quad (46)$$

The electric conductivity for the internode-scattering-induced current, whose detailed derivation can be found in Ref. [84], is given by

$$\begin{aligned} (\sigma_\chi^{\text{inter}})_{ij}(s) &= \frac{e^2 \rho_{-\chi}}{\rho_\chi \rho_G} \left[\tau_G - \frac{\tau \rho_G}{\rho_{-\chi}} \right] \int \frac{d^3\mathbf{k}}{(2\pi)^3} [-f_0'(\xi_\chi^s)] \left[(w_\chi^s)_i + (W_\chi^s)_i \right] \mathcal{I}_j^\chi, \\ \mathcal{I}^\chi &= \rho_\chi \langle \mathcal{D}_s^\chi \{ \mathbf{w}_\chi^s + \mathbf{W}_\chi^s \} \rangle = \sum_s \int \frac{d^3\mathbf{k}}{(2\pi)^3} [-f_0'(\xi_\chi^s(\mathbf{k}))] \{ \mathbf{w}_\chi^s + \mathbf{W}_\chi^s \}. \end{aligned} \quad (47)$$

We retain terms upto order B^2 by using Eq. (13). The above equation greatly simplifies for the cases when ε_s is a function of magnitudes of the momentum-components (i.e., $\varepsilon_s(\mathbf{k}) = \varepsilon_s(|k_x|, |k_y|, |k_z|)$). In that situation, $f_0'(\varepsilon_s(\mathbf{k}))$ and

its derivatives (with respect to ε_s) are even functions of \mathbf{k} . Hence, for our case of TSMs, we need to use

$$\begin{aligned}
(\sigma_\chi^{\text{inter}})_{ij}(s) &= \frac{e^2 \left[\tau_G \rho_{-\chi}^{(0)} - \tau \rho_G^{(0)} \right] \mathcal{Z}_{\chi,i}^s \zeta_j^\chi}{\rho_G^{(0)} \rho_\chi^{(0)}} + \mathcal{O}(B^3), \\
\rho_\chi^{(0)} &= \sum_{\bar{s}} \int \frac{d^3 \mathbf{q}}{(2\pi)^3} \left\{ -f'_0(\varepsilon_{\bar{s}}(\mathbf{q})) \right\} \Big|_{\text{node } \chi}, \quad \rho_G^{(0)} = \frac{\rho_\chi^{(0)} + \rho_{-\chi}^{(0)}}{2}, \quad \zeta_j^\chi = \sum_{\bar{s}} \mathcal{Z}_{\chi,j}^{\bar{s}}, \\
\mathcal{Z}_{\chi,j}^s &= B_j \int \frac{d^3 \mathbf{k}}{(2\pi)^3} \left[e \boldsymbol{\Omega}_\chi^s(\mathbf{k}) \cdot \mathbf{v}_s(\mathbf{k}) \left\{ -f'_0(\varepsilon_s(\mathbf{k})) \right\} + (m_\chi^s(\mathbf{k}))_j (v_s(\mathbf{k}))_j f''_0(\varepsilon_s(\mathbf{k})) \right] \Big|_{\text{node } \chi}. \tag{48}
\end{aligned}$$

Ref. [84] contains the resulting final expressions when we have the internode scatterings between (1) a single $J = 1$ TSM node (at the Γ -point) and a double-pseudospin-1/2 node (at the R -point); (2) a single RSW node (at the Γ -point) and a $J = 1$ double-TSM node (at the R -point).

For the special case where we have scatterings between two nodes of the same nature, with no net energy offset between the nodal points (relative to each other in the BZ), Eq. (48) further simplifies to [84]

$$(\sigma_\chi^{\text{inter}})_{ij}(s) = \frac{e^2 (\tau_G - \tau)}{\rho_1^{(0)}} \mathcal{Z}_{1,i}^s \sum_{\bar{s}} \mathcal{Z}_{1,j}^{\bar{s}}. \tag{49}$$

Here, we consider this situation involving the single band with $s = 1$ at each node of TSM, as shown in Fig. 4. Therefore, for our set-up, the nonzero components evaluate to

$$(\sigma_\chi^{\text{inter}})_{xx} = \frac{49 e^4 v_z J^3 \alpha_J^{\frac{2}{J}} (\tau_G - \tau) \Gamma(\frac{J+2}{2J})}{36 \pi^{\frac{5}{2}} E_F^{\frac{2}{J}}} B_x^2, \quad (\sigma_\chi^{\text{inter}})_{yx} = \frac{49 e^4 v_z J^3 \alpha_J^{\frac{2}{J}} (\tau_G - \tau) \Gamma(\frac{J+2}{2J})}{36 \pi^{\frac{5}{2}} E_F^{\frac{2}{J}}} B_x B_y. \tag{50}$$

Side by side, we invoke the analogous scenario with two conjugate nodes of the WSM/mWSM type, which gives us

$$(\sigma_\chi^{\text{inter}})_{xx} \Big|_{\text{mWSM}} = \frac{4 e^4 v_z J^3 \alpha_J^{\frac{2}{J}} (\tau_G - \tau) \Gamma(\frac{J+2}{2J})}{9 \pi^{\frac{5}{2}} E_F^{\frac{2}{J}}} B_x^2, \quad (\sigma_\chi^{\text{inter}})_{yx} \Big|_{\text{mWSM}} = \frac{4 e^4 v_z J^3 \alpha_J^{\frac{2}{J}} (\tau_G - \tau) \Gamma(\frac{J+2}{2J})}{9 \pi^{\frac{5}{2}} E_F^{\frac{2}{J}}} B_x B_y. \tag{51}$$

VI. SUMMARY, DISCUSSIONS, AND FUTURE PERSPECTIVES

As a follow-up of our investigations of transport signatures for twofold and multifold 3d semimetals, considering planar-Hall and planar-thermal Hall configurations, we have studied here nodes hosting pseudospin-1 quasiparticles. Resorting to the semiclassical Boltzmann equations and relaxation-time approximations, we have chalked out all the nonzero components of the linear-response tensors, assuming the weak (i.e., nonquantizing) magnetic-field limit. In order to have a complete description, we have incorporated the effects of both the Berry curvature and the orbital magnetic moment, since both of these arise from the underlying topological features of the bandstructure. Going beyond our previous works, we have computed the out-of-plane component of the electric conductivity, which are caused by the intrinsic anomalous-Hall and the Lorentz-force-contributed currents. It is evident from our results that the Lorentz-force operator gives rise to in-plane components, in addition to the out-of-plane ones. Last but not the least, we have worked out the response characteristics induced by internode scatterings. Our theoretical explorations involving TSMs are particularly important in the context of contemporary experiments, e.g., the one reported in Ref. [8]. In fact, we have elucidated the results upto $\mathcal{O}(B^3)$, because the data-fitting in Ref. [8] has been implemented via a phenomenological model (describing the $J = 1$ TSM) comprising terms upto order B^3 . Hence, the relevance and timeliness of our studies cannot be overemphasized.

The results for the in-plane components bear qualitative resemblance to those discussed in Ref. [33], which deals with WSMs and mWSMs (having twofold band-crossings). This is because, at the zeroth order in the OMM, the flat-band does not contribute to transport — hence, we have omitted their contributions, if any. The $J = 1$ case also resembles the RSW case, studied in Ref. [25], because both the systems are isotropic and have linear-in-momentum dispersions. In fact, here we have derived and compared some higher-order-in- \tilde{L} terms of an RSW node, in order to make a clear comparison between the characteristics for the $J = 1$ TSM case and the RSW case.

As emphasized above, we have here employed the relaxation-time approximations, both for the intranode- and internode-scattering processes. Hence, it remains to be seen if any new information is unravelled by going beyond the relaxation-time approximations [29, 97]. There are multiple other directions that can be pursued in the context of the studies reported here. One of those involves repeating our calculations in the presence of nonzero tilts of the TSM nodes [26, 29, 32, 34, 90, 98]. In particular, tilting causes linear-in- B terms to appear in the in-plane response coefficients, as found in Refs. [26, 32, 34, 90, 98]. In this connection, it is worth mentioning that a chiral pseudomagnetic field, induced by elastic deformations, can also give rise to B -linear terms, as elaborated on in earlier works [25, 30, 33, 83]. Next, it will

be worthwhile to study the transport properties under a strong quantizing magnetic field, when we will need to consider the energy levels being quantized into discrete Landau levels [47, 53, 54, 99]. Lastly, in order to simulate more realistic scenarios, we need to consider the effects of disorder and/or many-body interactions. This will necessitate incorporating state-of-the-art many-body formalisms [5, 7, 61, 100–104].

ACKNOWLEDGMENTS

We thank Rahul Ghosh for useful discussions.

Appendix A: Identities for some useful integrals

In order to solve the various conductivity expressions, we have to perform integrals of the form

$$\mathcal{I} = \int \frac{d^3 \mathbf{k}}{(2\pi)^3} \mathcal{T}(\mathbf{k}, \xi_\chi^s) f_0'(\xi_\chi^s), \quad (\text{A1})$$

where $\xi_\chi^s = \varepsilon_s(\mathbf{k}) + \varepsilon_\chi^{(m)}(\mathbf{k})$. Here, we focus only the cases when the chemical potential (μ) cuts the positive-energy band(s) and, therefore, $\varepsilon_s(\mathbf{k}) > 0$. Observing that the cylindrical symmetry of the system can be utilized to evaluate the integrals, we employ the following coordinate transformation:

$$k_x = \left(\frac{\varepsilon}{\alpha_J} \sin \gamma \right)^{1/J} \cos \phi, \quad k_y = \left(\frac{\varepsilon}{\alpha_J} \sin \gamma \right)^{1/J} \sin \phi, \quad k_z = \frac{\varepsilon}{v_z} \cos \gamma, \quad (\text{A2})$$

where $\varepsilon \in [0, \infty)$, $\phi \in [0, 2\pi)$, and $\gamma \in [0, \pi]$. The Jacobian for the transformation is $\mathcal{J}(\varepsilon, \gamma) = \frac{1}{J v_z \sin \gamma} \left(\frac{\varepsilon \sin \gamma}{\alpha_J} \right)^{2/J}$. We rewrite the integral using the following substitutions:

$$\int_{-\infty}^{\infty} d^3 \mathbf{k} \rightarrow \int_{-\infty}^{\infty} d\varepsilon \int_0^{2\pi} d\phi \int_0^\pi d\gamma \mathcal{J}(\varepsilon, \gamma) \quad \text{and} \quad \xi_\chi^s(\mathbf{k}) \rightarrow \xi_\chi^s(\varepsilon) = \varepsilon + \varepsilon_\chi^{(m)}. \quad (\text{A3})$$

With the implementation of the above coordinate transformation, the original integral evolves into

$$\begin{aligned} \mathcal{I} &= \frac{1}{(2\pi)^3} \int_{-\infty}^{\infty} d\varepsilon \int_0^{2\pi} d\phi \int_0^\pi d\gamma \mathcal{H}(\varepsilon, \phi, \gamma, \xi_\chi^s) f_0'(\xi_\chi^s) \quad [\text{where } \mathcal{H}(\varepsilon, \phi, \gamma, \xi_\chi^s) = \mathcal{J}(\varepsilon, \gamma) \mathcal{T}(\varepsilon, \phi, \gamma, \xi_\chi^s)] \\ &= \frac{1}{(2\pi)^3} \int_0^\infty d\varepsilon \mathcal{K}(\chi, \varepsilon) f_0'(\xi_\chi^s) \quad \left[\text{where } \mathcal{K}(\chi, \varepsilon) = \int_0^{2\pi} d\phi \int_0^\pi d\gamma \mathcal{H}(\varepsilon, \phi, \gamma, \xi_\chi^s) \right]. \end{aligned} \quad (\text{A4})$$

For the ε -integration, we apply the Sommerfeld expansion [89], which is valid under the condition $1/(\beta\mu) \ll 1$. This implies that we use the identity

$$\int_0^\infty d\varepsilon \varepsilon^n [-f_0'(\varepsilon)] = \Upsilon_n(\mu) = \mu^n \left[1 + \frac{\pi^2 n(n-1)}{6(\beta\mu)^2} + \mathcal{O}((\beta\mu)^{-3}) \right], \quad (\text{A5})$$

where $\beta(\mathbf{r}) = 1/T(\mathbf{r})$.

For integrals involving higher-order derivatives of f_0 , we have

$$\int_0^\infty d\varepsilon \varepsilon^n (-1)^{\lambda+1} \frac{\partial^{\lambda+1} f_0(\varepsilon)}{\partial \varepsilon^{\lambda+1}} = \frac{n!}{(n-\lambda)!} \Upsilon_{n-\lambda}(\mu). \quad (\text{A6})$$

For the thermoelectric and thermal tensors, we need to use the identity

$$\int_0^\infty d\varepsilon \varepsilon^n (\varepsilon - \mu) (-1)^{\lambda+1} \frac{\partial^{\lambda+1} f_0(\varepsilon)}{\partial \varepsilon^{\lambda+1}} = \frac{(n+1)!}{(n+1-\lambda)!} \Upsilon_{n+1-\lambda}(\mu) - \mu \frac{n!}{(n-\lambda)!} \Upsilon_{n-\lambda}(\mu). \quad (\text{A7})$$

Appendix B: Current from the Lorentz-force part

In this appendix, we deal with the so-called Lorentz-force part, which arises from the current density of (see Refs. [25, 90] for a detailed derivation)

$$\begin{aligned} \mathbf{J}_\chi^{s, \text{LF}} &= -e^2 \tau \int \frac{d^3 \mathbf{k}}{(2\pi)^3} (\mathbf{w}_\chi^s + \mathbf{W}_\chi^s) f_0'(\xi_\chi^s) \mathcal{Y}_\chi^s, \quad \text{where } \check{L} = (\mathbf{w}_\chi^s \times \mathbf{B}) \cdot \nabla_{\mathbf{k}}, \\ \mathbf{W}_\chi^s &= e (\mathbf{w}_\chi^s \cdot \boldsymbol{\Omega}_\chi^s) \mathbf{B}, \quad \mathcal{Y}_\chi^s = \sum_{n=1}^{\infty} (e\tau \mathcal{D}_\chi^s)^n \check{L}^n [\mathcal{D}_\chi^s \{ \mathbf{w}_\chi^s + \mathbf{W}_\chi^s \} \cdot \mathbf{E}]. \end{aligned} \quad (\text{B1})$$

This part arises from the action of the Lorentz-force operator \check{L} . The nomenclature reflects the fact that it includes the classical Hall effect due to the Lorentz force. The corresponding components of the electric conductivity is

$$(\sigma_{\chi}^{\text{LF}})_{ij}(s) = -e^2 \tau \int \frac{d^3 \mathbf{k}}{(2\pi)^3} [(w_{\chi}^s)_i + (W_{\chi}^s)_i] f'_0(\xi_{\chi}^s) \frac{\partial \mathcal{Y}_{\chi}^s}{\partial E_j}. \quad (\text{B2})$$

The solution is obtained by taking the terms in the summation upto a chosen value of n and, thereafter, expanding the expressions upto the desired power in B .

1. $n = 1$: Terms originating from the linear action of the Lorentz-force operator

The $n = 1$ term leads to the current density of

$$\begin{aligned} \mathbf{J}_{\chi}^{s,\text{LF}} &= -e^3 \tau^2 \int \frac{d^3 \mathbf{k}}{(2\pi)^3} [\mathbf{w}_{\chi}^s + \mathbf{W}_{\chi}^s] \mathcal{D}_{\chi}^s f'_0(\xi_{\chi}^s) (t_1 + t_2), \\ t_1 &= \mathcal{D}_{\chi}^s \check{L} [\{\mathbf{w}_{\chi}^s + \mathbf{W}_{\chi}^s\} \cdot \mathbf{E}], \quad t_2 = [\{\mathbf{w}_{\chi}^s + \mathbf{W}_{\chi}^s\} \cdot \mathbf{E}] \check{L} \mathcal{D}_{\chi}^s. \end{aligned} \quad (\text{B3})$$

Expanding the integrand upto $\mathcal{O}(B^3)$, we obtain

$$\begin{aligned} t_1 &= \{1 - e(\boldsymbol{\Omega}_{\chi}^s \cdot \mathbf{B}) + e^2(\boldsymbol{\Omega}_{\chi}^s \cdot \mathbf{B})^2\} (\mathbf{v}_s \times \mathbf{B}) \cdot \nabla_{\mathbf{k}} (\mathbf{v}_s \cdot \mathbf{E}) + (\mathbf{v}_s \times \mathbf{B}) \cdot \nabla_{\mathbf{k}} (U_{\chi}^{(m)} \cdot \mathbf{E}) \\ &\quad + \{1 - e(\boldsymbol{\Omega}_{\chi}^s \cdot \mathbf{B})\} (\mathbf{v}_s \times \mathbf{B}) \cdot \nabla_{\mathbf{k}} [(\mathbf{u}_{\chi}^{(m)} + \mathbf{V}_{\chi}^s) \cdot \mathbf{E}] + (\mathbf{u}_{\chi}^{(m)} \times \mathbf{B}) \cdot \nabla_{\mathbf{k}} [(\mathbf{u}_{\chi}^{(m)} + \mathbf{V}_{\chi}^s) \cdot \mathbf{E}] \\ &\quad + \{1 - e(\boldsymbol{\Omega}_{\chi}^s \cdot \mathbf{B})\} (\mathbf{u}_{\chi}^{(m)} \times \mathbf{B}) \cdot \nabla_{\mathbf{k}} (\mathbf{v}_s \cdot \mathbf{E}), \end{aligned} \quad (\text{B4})$$

and

$$\begin{aligned} t_2 &= (\mathbf{v}_s \cdot \mathbf{E}) (\mathbf{v}_s \times \mathbf{B}) \cdot \nabla_{\mathbf{k}} [-e(\boldsymbol{\Omega}_{\chi}^s \cdot \mathbf{B}) + e^2(\boldsymbol{\Omega}_{\chi}^s \cdot \mathbf{B})^2] + (\mathbf{v}_s \cdot \mathbf{E}) (\mathbf{u}_{\chi}^{(m)} \times \mathbf{B}) \cdot \nabla_{\mathbf{k}} [-e(\boldsymbol{\Omega}_{\chi}^s \cdot \mathbf{B})] \\ &\quad + (\mathbf{u}_{\chi}^{(m)} + \mathbf{V}_{\chi}^s) \cdot \mathbf{E} (\mathbf{v}_s \times \mathbf{B}) \cdot \nabla_{\mathbf{k}} [-e(\boldsymbol{\Omega}_{\chi}^s \cdot \mathbf{B})]. \end{aligned} \quad (\text{B5})$$

Let us express the current density as

$$\mathbf{J}_{\chi}^{s,\text{LF}} = -e^3 \tau^2 \int \frac{d^3 \mathbf{k}}{(2\pi)^3} \sum_{\delta=1}^3 \mathcal{N}_{1,\delta}, \quad (\text{B6})$$

where $\mathcal{N}_{1,\delta}$ has a B^{δ} -dependence. These evaluate to the following expressions:

1. Linear-in- B :

$$\mathcal{N}_{1,1} = \mathbf{v}_s f'_0(\varepsilon_s) (\mathbf{v}_s \times \mathbf{B}) \cdot \nabla_{\mathbf{k}} (\mathbf{v}_s \cdot \mathbf{E}). \quad (\text{B7})$$

2. Quadratic-in- B :

$$\begin{aligned} \mathcal{N}_{1,2} &= \mathbf{v}_s (\mathbf{v}_s \cdot \mathbf{E}) f'_0(\varepsilon_s) (\mathbf{v}_s \times \mathbf{B}) \cdot \nabla_{\mathbf{k}} [-e(\boldsymbol{\Omega}_{\chi}^s \cdot \mathbf{B})] + \mathbf{v}_s f'_0(\varepsilon_s) (\mathbf{v}_s \times \mathbf{B}) \cdot \nabla_{\mathbf{k}} [(\mathbf{u}_{\chi}^{(m)} + \mathbf{V}_{\chi}^s) \cdot \mathbf{E}] \\ &\quad + \left[\{-2e(\boldsymbol{\Omega}_{\chi}^s \cdot \mathbf{B}) \mathbf{v}_s + (\mathbf{u}_{\chi}^{(m)} + \mathbf{V}_{\chi}^s)\} f'_0(\varepsilon_s) - (\mathbf{m}_{\chi}^s \cdot \mathbf{B}) \mathbf{v}_s f''_0(\varepsilon_s) \right] (\mathbf{v}_s \times \mathbf{B}) \cdot \nabla_{\mathbf{k}} (\mathbf{v}_s \cdot \mathbf{E}) \\ &\quad + \mathbf{v}_s f'_0(\varepsilon_s) (\mathbf{u}_{\chi}^{(m)} \times \mathbf{B}) \cdot \nabla_{\mathbf{k}} (\mathbf{v}_s \cdot \mathbf{E}). \end{aligned} \quad (\text{B8})$$

3. Cubic-in- B :

$$\begin{aligned} \mathcal{N}_{1,3} &= \left[\{-e(\boldsymbol{\Omega}_{\chi}^s \cdot \mathbf{B}) \mathbf{v}_s (\mathbf{v}_s \cdot \mathbf{E}) + \mathbf{v}_s (\mathbf{u}_{\chi}^{(m)} + \mathbf{V}_{\chi}^s) \cdot \mathbf{E} + (\mathbf{v}_s \cdot \mathbf{E}) (\mathbf{u}_{\chi}^{(m)} + \mathbf{V}_{\chi}^s)\} f'_0(\varepsilon_s) - (\mathbf{m}_{\chi}^s \cdot \mathbf{B}) \mathbf{v}_s (\mathbf{v}_s \cdot \mathbf{E}) f''_0(\varepsilon_s) \right] \\ &\quad \times [(\mathbf{v}_s \times \mathbf{B}) \cdot \nabla_{\mathbf{k}} \{-e(\boldsymbol{\Omega}_{\chi}^s \cdot \mathbf{B})\}] \\ &\quad + \mathbf{v}_s (\mathbf{v}_s \cdot \mathbf{E}) f'_0(\varepsilon_s) [(\mathbf{v}_s \times \mathbf{B}) \cdot \nabla_{\mathbf{k}} [e^2(\boldsymbol{\Omega}_{\chi}^s \cdot \mathbf{B})^2] + (\mathbf{u}_{\chi}^{(m)} \times \mathbf{B}) \cdot \nabla_{\mathbf{k}} \{-e(\boldsymbol{\Omega}_{\chi}^s \cdot \mathbf{B})\}] \\ &\quad + \left[\{3e^2(\boldsymbol{\Omega}_{\chi}^s \cdot \mathbf{B})^2 \mathbf{v}_s - 2e(\boldsymbol{\Omega}_{\chi}^s \cdot \mathbf{B}) (\mathbf{u}_{\chi}^{(m)} + \mathbf{V}_{\chi}^s) + U_{\chi}^{(m)}\} f'_0(\varepsilon_s) \right. \\ &\quad \left. + \left\{ 2e(\boldsymbol{\Omega}_{\chi}^s \cdot \mathbf{B}) \mathbf{v}_s - (\mathbf{u}_{\chi}^{(m)} + \mathbf{V}_{\chi}^s) \right\} (\mathbf{m}_{\chi}^s \cdot \mathbf{B}) f''_0(\varepsilon_s) + \frac{(\mathbf{m}_{\chi}^s \cdot \mathbf{B})^2}{2} \mathbf{v}_s f'''_0(\varepsilon_s) \right] (\mathbf{v}_s \times \mathbf{B}) \cdot \nabla_{\mathbf{k}} (\mathbf{v}_s \cdot \mathbf{E}) \\ &\quad + \left[\{-2e(\boldsymbol{\Omega}_{\chi}^s \cdot \mathbf{B}) \mathbf{v}_s + (\mathbf{u}_{\chi}^{(m)} + \mathbf{V}_{\chi}^s)\} f'_0(\varepsilon_s) - (\mathbf{m}_{\chi}^s \cdot \mathbf{B}) \mathbf{v}_s f''_0(\varepsilon_s) \right] \\ &\quad \times [(\mathbf{v}_s \times \mathbf{B}) \cdot \nabla_{\mathbf{k}} \{(\mathbf{u}_{\chi}^{(m)} + \mathbf{V}_{\chi}^s) \cdot \mathbf{E}\} + (\mathbf{u}_{\chi}^{(m)} \times \mathbf{B}) \cdot \nabla_{\mathbf{k}} (\mathbf{v}_s \cdot \mathbf{E})] \\ &\quad + \mathbf{v}_s f'_0(\varepsilon_s) [(\mathbf{v}_s \times \mathbf{B}) \cdot \nabla_{\mathbf{k}} (U_{\chi}^{(m)} \cdot \mathbf{E}) + (\mathbf{u}_{\chi}^{(m)} \times \mathbf{B}) \cdot \nabla_{\mathbf{k}} \{(\mathbf{u}_{\chi}^{(m)} + \mathbf{V}_{\chi}^s) \cdot \mathbf{E}\}]. \end{aligned} \quad (\text{B9})$$

2. $n = 2$: Terms originating from the quadratic action of the Lorentz-force operator

The $n = 2$ term leads to the current density of

$$\mathbf{J}_\chi^{s,\text{LF}} = -e^4 \tau^3 \int \frac{d^3 \mathbf{k}}{(2\pi)^3} \{\mathbf{w}_\chi^s + \mathbf{W}_\chi^s\} (\mathcal{D}_\chi^s)^2 f'_0(\xi_\chi^s) \check{L}^2 [\mathcal{D}_\chi^s \{\mathbf{w}_\chi^s + \mathbf{W}_\chi^s\} \cdot \mathbf{E}]. \quad (\text{B10})$$

Due to the presence of \check{L}^2 , there is no linear-in- B term here. Let us express the current density as

$$\mathbf{J}_\chi^{s,\text{LF}} = -e^4 \tau^3 \int \frac{d^3 \mathbf{k}}{(2\pi)^3} \sum_{\delta=2}^3 \mathcal{N}_{2,\delta}, \quad (\text{B11})$$

where $\mathcal{N}_{2,\delta}$ has a B^δ -dependence. These evaluate to the following expressions:

1. Quadratic-in- B :

$$\mathcal{N}_{2,2} = \mathbf{v}_s f'_0(\varepsilon_s) (\mathbf{v}_s \times \mathbf{B}) \cdot \nabla_{\mathbf{k}} [(\mathbf{v}_s \times \mathbf{B}) \cdot \nabla_{\mathbf{k}} (\mathbf{v}_s \cdot \mathbf{E})]. \quad (\text{B12})$$

2. Cubic-in- B :

$$\begin{aligned} \mathcal{N}_{2,3} = & \mathbf{v}_s f'_0(\varepsilon_s) (\mathbf{v}_s \times \mathbf{B}) \cdot \nabla_{\mathbf{k}} \left[-e (\boldsymbol{\Omega}_\chi^s \cdot \mathbf{B}) (\mathbf{v}_s \times \mathbf{B}) \cdot \nabla_{\mathbf{k}} (\mathbf{v}_s \cdot \mathbf{E}) + (\mathbf{v}_s \times \mathbf{B}) \cdot \nabla_{\mathbf{k}} \left\{ \left(\mathbf{u}_\chi^{(m)} + \mathbf{V}_\chi^s \right) \cdot \mathbf{E} \right\} \right. \\ & \left. + \left(\mathbf{u}_\chi^{(m)} \times \mathbf{B} \right) \cdot \nabla_{\mathbf{k}} (\mathbf{v}_s \cdot \mathbf{E}) \right] \\ & + \mathbf{v}_s f'_0(\varepsilon_s) \left(\mathbf{u}_\chi^{(m)} \times \mathbf{B} \right) \cdot \nabla_{\mathbf{k}} [(\mathbf{v}_s \times \mathbf{B}) \cdot \nabla_{\mathbf{k}} (\mathbf{v}_s \cdot \mathbf{E})] \\ & + \mathbf{v}_s f'_0(\varepsilon_s) (\mathbf{v}_s \times \mathbf{B}) \cdot \nabla_{\mathbf{k}} [(\mathbf{v}_s \cdot \mathbf{E}) (\mathbf{v}_s \times \mathbf{B}) \cdot \nabla_{\mathbf{k}} \{-e (\boldsymbol{\Omega}_\chi^s \cdot \mathbf{B})\}] \\ & + \left[\left\{ -2e \mathbf{v}_s (\boldsymbol{\Omega}_\chi^s \cdot \mathbf{B}) + \mathbf{u}_\chi^{(m)} + \mathbf{V}_\chi^s \right\} f'_0(\varepsilon_s) - (\mathbf{m}_\chi^s \cdot \mathbf{B}) \mathbf{v}_s f''_0(\varepsilon_s) \right] (\mathbf{v}_s \times \mathbf{B}) \cdot [\nabla_{\mathbf{k}} \{(\mathbf{v}_s \times \mathbf{B}) \cdot \nabla_{\mathbf{k}} (\mathbf{v}_s \cdot \mathbf{E})\}]. \end{aligned} \quad (\text{B13})$$

3. $n = 3$: Terms originating from the cubic action of the Lorentz-force operator

The $n = 3$ term leads to the current density of

$$\mathbf{J}_\chi^{s,\text{LF}} = -e^5 \tau^4 \int \frac{d^3 \mathbf{k}}{(2\pi)^3} \{\mathbf{w}_\chi^s + \mathbf{W}_\chi^s\} (\mathcal{D}_\chi^s)^3 f'_0(\xi_\chi^s) \check{L}^3 [\mathcal{D}_\chi^s \{\mathbf{w}_\chi^s + \mathbf{W}_\chi^s\} \cdot \mathbf{E}]. \quad (\text{B14})$$

Due to the presence of \check{L}^3 , only a cubic-in- B term needs to be extracted here. We can express the current density as

$$\mathbf{J}_\chi^{s,\text{LF}} = -e^5 \tau^4 \int \frac{d^3 \mathbf{k}}{(2\pi)^3} \mathcal{N}_{3,3}, \quad \text{where } \mathcal{N}_{3,3} = \mathbf{v}_s f'_0(\varepsilon_s) (\mathbf{v}_s \times \mathbf{B}) \cdot \nabla_{\mathbf{k}} [(\mathbf{v}_s \times \mathbf{B}) \cdot \nabla_{\mathbf{k}} \{(\mathbf{v}_s \times \mathbf{B}) \cdot \nabla_{\mathbf{k}} (\mathbf{v}_s \cdot \mathbf{E})\}]. \quad (\text{B15})$$

-
- [1] A. A. Burkov and L. Balents, Weyl semimetal in a topological insulator multilayer, *Phys. Rev. Lett.* **107**, 127205 (2011).
 - [2] B. Yan and C. Felser, Topological materials: Weyl semimetals, *Annual Rev. of Condensed Matter Phys.* **8**, 337 (2017).
 - [3] I. Mandal and K. Saha, Thermoelectric response in nodal-point semimetals, *Ann. Phys. (Berlin)* **536**, 2400016 (2024).
 - [4] B. Bradlyn, J. Cano, Z. Wang, M. G. Vergniory, C. Felser, R. J. Cava, and B. A. Bernevig, Beyond Dirac and Weyl fermions: Unconventional quasiparticles in conventional crystals, *Science* **353** (2016).
 - [5] I. Mandal, Robust marginal Fermi liquid in birefringent semimetals, *Phys. Lett. A* **418**, 127707 (2021).
 - [6] F. Flicker, F. de Juan, B. Bradlyn, T. Morimoto, M. G. Vergniory, and A. G. Grushin, Chiral optical response of multifold fermions, *Phys. Rev. B* **98**, 155145 (2018).
 - [7] I. Mandal and H. Freire, Transport properties in non-Fermi liquid phases of nodal-point semimetals, *Journal of Physics: Condensed Matter* **36**, 443002 (2024).
 - [8] F. Balduini, A. Molinari, L. Rocchino, V. Hasse, C. Felser, M. Sousa, C. Zota, H. Schmid, A. G. Grushin, and B. Gotsmann, Intrinsic negative magnetoresistance from the chiral anomaly of multifold fermions, *Nature Communications* **15**, 6526 (2024).
 - [9] N. P. Armitage, E. J. Mele, and A. Vishwanath, Weyl and Dirac semimetals in three-dimensional solids, *Rev. Mod. Phys.* **90**, 015001 (2018).
 - [10] I. Mandal, Transmission in pseudospin-1 and pseudospin-3/2 semimetals with linear dispersion through scalar and vector potential barriers, *Phys. Lett. A* **384**, 126666 (2020).

- [11] I. C. Fulga and A. Stern, Triple point fermions in a minimal symmorphic model, *Phys. Rev. B* **95**, 241116 (2017).
- [12] S. Nandy, K. Sengupta, and D. Sen, Transport across junctions of pseudospin-one fermions, *Phys. Rev. B* **100**, 085134 (2019).
- [13] S. Sekh and I. Mandal, Circular dichroism as a probe for topology in three-dimensional semimetals, *Phys. Rev. B* **105**, 235403 (2022).
- [14] P. Tang, Q. Zhou, and S.-C. Zhang, Multiple types of topological fermions in transition metal silicides, *Phys. Rev. Lett.* **119**, 206402 (2017).
- [15] Y. Shen, Y. Jin, Y. Ge, M. Chen, and Z. Zhu, Chiral topological metals with multiple types of quasiparticle fermions and large spin Hall effect in the SrGePt family materials, *Phys. Rev. B* **108**, 035428 (2023).
- [16] I. Mandal, Nature of Andreev bound states in Josephson junctions of triple-point semimetals, *arXiv e-prints* (2024), [arXiv:2406.15350 \[cond-mat.supr-con\]](https://arxiv.org/abs/2406.15350).
- [17] L. Liang and Y. Yu, Semimetal with both Rarita-Schwinger-Weyl and Weyl excitations, *Phys. Rev. B* **93**, 045113 (2016).
- [18] I. Boettcher, Interplay of topology and electron-electron interactions in Rarita-Schwinger-Weyl semimetals, *Phys. Rev. Lett.* **124**, 127602 (2020).
- [19] J. M. Link, I. Boettcher, and I. F. Herbut, *d*-wave superconductivity and Bogoliubov-Fermi surfaces in Rarita-Schwinger-Weyl semimetals, *Phys. Rev. B* **101**, 184503 (2020).
- [20] H. Isobe and L. Fu, Quantum critical points of $j = \frac{3}{2}$ Dirac electrons in antiperovskite topological crystalline insulators, *Phys. Rev. B* **93**, 241113 (2016).
- [21] J.-Z. Ma, Q.-S. Wu, M. Song, S.-N. Zhang, E. Guedes, S. Ekahana, M. Krivenkov, M. Yao, S.-Y. Gao, W.-H. Fan, *et al.*, Observation of a singular Weyl point surrounded by charged nodal walls in ptga, *Nature Communications* **12**, 3994 (2021).
- [22] S. Sekh and I. Mandal, Magnus Hall effect in three-dimensional topological semimetals, *Eur. Phys. J. Plus* **137**, 736 (2022).
- [23] I. Mandal, Transmission and conductance across junctions of isotropic and anisotropic three-dimensional semimetals, *Eur. Phys. J. Plus* **138**, 1039 (2023).
- [24] I. Mandal, Andreev bound states in superconductor-barrier-superconductor junctions of Rarita-Schwinger-Weyl semimetals, *Phys. Lett. A* **503**, 129410 (2024).
- [25] R. Ghosh, F. Haidar, and I. Mandal, Linear response in planar Hall and thermal Hall setups for Rarita-Schwinger-Weyl semimetals, *Phys. Rev. B* **110**, 245113 (2024).
- [26] I. Mandal, S. Saha, and R. Ghosh, Signatures of topology in generic transport measurements for Rarita-Schwinger-Weyl semimetals, *Solid State Communications* **397**, 115799 (2025).
- [27] D. Xiao, M.-C. Chang, and Q. Niu, Berry phase effects on electronic properties, *Rev. Mod. Phys.* **82**, 1959 (2010).
- [28] G. Sundaram and Q. Niu, Wave-packet dynamics in slowly perturbed crystals: Gradient corrections and Berry-phase effects, *Phys. Rev. B* **59**, 14915 (1999).
- [29] A. Knoll, C. Timm, and T. Meng, Negative longitudinal magnetoconductance at weak fields in Weyl semimetals, *Phys. Rev. B* **101**, 201402 (2020).
- [30] R. Ghosh and I. Mandal, Electric and thermoelectric response for Weyl and multi-Weyl semimetals in planar Hall configurations including the effects of strain, *Physica E: Low-dimensional Systems and Nanostructures* **159**, 115914 (2024).
- [31] A. Graf and F. Piéchon, Berry curvature and quantum metric in *N*-band systems: An eigenprojector approach, *Phys. Rev. B* **104**, 085114 (2021).
- [32] R. Ghosh and I. Mandal, Direction-dependent conductivity in planar Hall set-ups with tilted Weyl/multi-Weyl semimetals, *Journal of Physics: Condensed Matter* **36**, 275501 (2024).
- [33] L. Medel, R. Ghosh, A. Martín-Ruiz, and I. Mandal, Electric, thermal, and thermoelectric magnetoconductivity for Weyl/multi-Weyl semimetals in planar Hall set-ups induced by the combined effects of topology and strain, *Scientific Reports* **14**, 21390 (2024).
- [34] I. Mandal, Anisotropic conductivity for the type-I and type-II phases of Weyl/multi-Weyl semimetals in planar Hall set-ups, *arXiv e-prints* (2024), [arXiv:2410.05028 \[cond-mat.mes-hall\]](https://arxiv.org/abs/2410.05028).
- [35] F. D. M. Haldane, Berry curvature on the Fermi surface: Anomalous Hall effect as a topological Fermi-liquid property, *Phys. Rev. Lett.* **93**, 206602 (2004).
- [36] P. Goswami and S. Tewari, Axionic field theory of (3 + 1)-dimensional Weyl semimetals, *Phys. Rev. B* **88**, 245107 (2013).
- [37] A. A. Burkov, Anomalous Hall effect in Weyl metals, *Phys. Rev. Lett.* **113**, 187202 (2014).
- [38] S.-B. Zhang, H.-Z. Lu, and S.-Q. Shen, Linear magnetoconductivity in an intrinsic topological Weyl semimetal, *New Journal of Phys.* **18**, 053039 (2016).
- [39] Q. Chen and G. A. Fiete, Thermoelectric transport in double-Weyl semimetals, *Phys. Rev. B* **93**, 155125 (2016).
- [40] S. Nandy, G. Sharma, A. Taraphder, and S. Tewari, Chiral anomaly as the origin of the planar Hall effect in Weyl semimetals, *Phys. Rev. Lett.* **119**, 176804 (2017).
- [41] S. Nandy, A. Taraphder, and S. Tewari, Berry phase theory of planar Hall effect in topological insulators, *Scientific Reports* **8**, 14983 (2018).
- [42] K. Das and A. Agarwal, Linear magnetochiral transport in tilted type-I and type-II Weyl semimetals, *Phys. Rev. B* **99**, 085405 (2019).
- [43] K. Das and A. Agarwal, Thermal and gravitational chiral anomaly induced magneto-transport in Weyl semimetals, *Phys. Rev. Res.* **2**, 013088 (2020).
- [44] S. Das, K. Das, and A. Agarwal, Nonlinear magnetoconductivity in Weyl and multi-Weyl semimetals in quantizing magnetic field, *Phys. Rev. B* **105**, 235408 (2022).
- [45] O. Pal, B. Dey, and T. K. Ghosh, Berry curvature induced magnetotransport in 3D noncentrosymmetric metals, *Journal of Phys.: Condensed Matter* **34**, 025702 (2022).
- [46] O. Pal, B. Dey, and T. K. Ghosh, Berry curvature induced anisotropic magnetotransport in a quadratic triple-component fermionic system, *Journal of Phys.: Condensed Matter* **34**, 155702 (2022).
- [47] L. X. Fu and C. M. Wang, Thermoelectric transport of multi-Weyl semimetals in the quantum limit, *Phys. Rev. B* **105**, 035201 (2022).

- [48] Y. Araki, Magnetic textures and dynamics in magnetic Weyl semimetals, *Ann. Phys. (Berlin)* **532**, 1900287 (2020).
- [49] Y. P. Mizuta and F. Ishii, Contribution of Berry curvature to thermoelectric effects, *Proceedings of the International Conference on Strongly Correlated Electron Systems (SCES2013)*, *JPS Conf. Proc.* **3**, 017035 (2014).
- [50] S. Yadav, S. Fazzini, and I. Mandal, Magneto-transport signatures in periodically-driven Weyl and multi-Weyl semimetals, *Physica E Low-Dimensional Systems and Nanostructures* **144**, 115444 (2022).
- [51] L. Li, J. Cao, C. Cui, Z.-M. Yu, and Y. Yao, Planar Hall effect in topological Weyl and nodal-line semimetals, *Phys. Rev. B* **108**, 085120 (2023).
- [52] V. Gusynin, S. Sharapov, and J. Carbotte, Magneto-optical conductivity in graphene, *Journal of Phys.: Condensed Matter* **19**, 026222 (2006).
- [53] M. Stålhammar, J. Larana-Aragon, J. Knolle, and E. J. Bergholtz, Magneto-optical conductivity in generic Weyl semimetals, *Phys. Rev. B* **102**, 235134 (2020).
- [54] S. Yadav, S. Sekh, and I. Mandal, Magneto-optical conductivity in the type-I and type-II phases of Weyl/multi-Weyl semimetals, *Physica B: Condensed Matter* **656**, 414765 (2023).
- [55] M. Papaž and L. Fu, Magnus Hall effect, *Phys. Rev. Lett.* **123**, 216802 (2019).
- [56] D. Mandal, K. Das, and A. Agarwal, Magnus Nernst and thermal Hall effect, *Phys. Rev. B* **102**, 205414 (2020).
- [57] I. Mandal, Signatures of two- and three-dimensional semimetals from circular dichroism, *International Journal of Modern Physics B* **38**, 2450216 (2024).
- [58] J. E. Moore, Optical properties of Weyl semimetals, *National Science Rev.* **6**, 206 (2018).
- [59] C. Guo, V. S. Asadchy, B. Zhao, and S. Fan, Light control with Weyl semimetals, *eLight* **3**, 2 (2023).
- [60] A. Avdoshkin, V. Kozii, and J. E. Moore, Interactions remove the quantization of the chiral photocurrent at Weyl points, *Phys. Rev. Lett.* **124**, 196603 (2020).
- [61] I. Mandal, Effect of interactions on the quantization of the chiral photocurrent for double-Weyl semimetals, *Symmetry* **12** (2020).
- [62] I. Mandal and A. Sen, Tunneling of multi-Weyl semimetals through a potential barrier under the influence of magnetic fields, *Phys. Lett. A* **399**, 127293 (2021).
- [63] S. Bera and I. Mandal, Floquet scattering of quadratic band-touching semimetals through a time-periodic potential well, *Journal of Phys. Condensed Matter* **33**, 295502 (2021).
- [64] S. Bera, S. Sekh, and I. Mandal, Floquet transmission in Weyl/multi-Weyl and nodal-line semimetals through a time-periodic potential well, *Ann. Phys. (Berlin)* **535**, 2200460 (2023).
- [65] J. Cayssol and J. N. Fuchs, Topological and geometrical aspects of band theory, *Journal of Physics: Materials* **4**, 034007 (2021).
- [66] M. M. H. Polash, S. Yalameha, H. Zhou, K. Ahadi, Z. Nourbakhsh, and D. Vashaee, Topological quantum matter to topological phase conversion: Fundamentals, materials, physical systems for phase conversions, and device applications, *Materials Science and Engineering: R: Reports* **145**, 100620 (2021).
- [67] H. Nielsen and M. Ninomiya, A no-go theorem for regularizing chiral fermions, *Phys. Lett. B* **105**, 219 (1981).
- [68] D. Bercioux, D. F. Urban, H. Grabert, and W. Häusler, Massless Dirac-Weyl fermions in a \mathcal{T}_3 optical lattice, *Phys. Rev. A* **80**, 063603 (2009).
- [69] N. Goldman, D. F. Urban, and D. Bercioux, Topological phases for fermionic cold atoms on the Lieb lattice, *Phys. Rev. A* **83**, 063601 (2011).
- [70] Y.-Q. Zhu, D.-W. Zhang, H. Yan, D.-Y. Xing, and S.-L. Zhu, Emergent pseudospin-1 Maxwell fermions with a threefold degeneracy in optical lattices, *Phys. Rev. A* **96**, 033634 (2017).
- [71] B. Q. Lv, Z.-L. Feng, J.-Z. Zhao, N. F. Q. Yuan, A. Zong, K. F. Luo, R. Yu, Y.-B. Huang, V. N. Strocov, A. Chikina, A. A. Soluyanov, N. Gedik, Y.-G. Shi, T. Qian, and H. Ding, Observation of multiple types of topological fermions in PdBiSe, *Phys. Rev. B* **99**, 241104 (2019).
- [72] Z. Zhu, G. W. Winkler, Q. Wu, J. Li, and A. A. Soluyanov, Triple point topological metals, *Phys. Rev. X* **6**, 031003 (2016).
- [73] H. Weng, C. Fang, Z. Fang, and X. Dai, Topological semimetals with triply degenerate nodal points in θ -phase tantalum nitride, *Phys. Rev. B* **93**, 241202 (2016).
- [74] P. Tang, Q. Zhou, and S.-C. Zhang, Multiple types of topological fermions in transition metal silicides, *Phys. Rev. Lett.* **119**, 206402 (2017).
- [75] H. Weng, C. Fang, Z. Fang, and X. Dai, Coexistence of Weyl fermion and massless triply degenerate nodal points, *Phys. Rev. B* **94**, 165201 (2016).
- [76] R. Shen, L. B. Shao, B. Wang, and D. Y. Xing, Single Dirac cone with a flat band touching on line-centered-square optical lattices, *Phys. Rev. B* **81**, 041410 (2010).
- [77] Z. Lan, N. Goldman, A. Bermudez, W. Lu, and P. Öhberg, Dirac-Weyl fermions with arbitrary spin in two-dimensional optical superlattices, *Phys. Rev. B* **84**, 165115 (2011).
- [78] D. F. Urban, D. Bercioux, M. Wimmer, and W. Häusler, Barrier transmission of Dirac-like pseudospin-one particles, *Phys. Rev. B* **84**, 115136 (2011).
- [79] P. He, X. Shen, D.-W. Zhang, and S.-L. Zhu, Simulating the Klein tunneling of pseudospin-one Maxwell particles with trapped ions, *Physics Letters A* **383**, 2462 (2019).
- [80] H.-Y. Xu and Y.-C. Lai, Revival resonant scattering, perfect caustics, and isotropic transport of pseudospin-1 particles, *Phys. Rev. B* **94**, 165405 (2016).
- [81] S. Nandy, S. Manna, D. Călugăru, and B. Roy, Generalized triple-component fermions: Lattice model, Fermi arcs, and anomalous transport, *Phys. Rev. B* **100**, 235201 (2019).
- [82] C. Fang, M. J. Gilbert, X. Dai, and B. A. Bernevig, Multi-Weyl topological semimetals stabilized by point group symmetry, *Phys. Rev. Lett.* **108**, 266802 (2012).
- [83] L. Medel Onofre and A. Martín-Ruiz, Planar Hall effect in Weyl semimetals induced by pseudoelectromagnetic fields, *Phys. Rev. B* **108**, 155132 (2023).

- [84] I. Mandal, Chiral anomaly and internode scatterings in multifold semimetals, [arXiv e-prints \(2024\)](#), [arXiv:2411.18434 \[cond-mat.mes-hall\]](#).
- [85] G. Chang, S.-Y. Xu, B. J. Wieder, D. S. Sanchez, S.-M. Huang, I. Belopolski, T.-R. Chang, S. Zhang, A. Bansil, H. Lin, and M. Z. Hasan, Unconventional chiral fermions and large topological Fermi arcs in RhSi, *Phys. Rev. Lett.* **119**, 206401 (2017).
- [86] K. Nakazawa, T. Yamaguchi, and A. Yamakage, Nonlinear charge and thermal transport properties induced by orbital magnetic moment in chiral crystal cobalt monosilicide, [arXiv e-prints \(2024\)](#), [arXiv:2409.08040 \[cond-mat.str-el\]](#).
- [87] D. Xiao, W. Yao, and Q. Niu, Valley-contrasting physics in graphene: Magnetic moment and topological transport, *Phys. Rev. Lett.* **99**, 236809 (2007).
- [88] J. Xiong, S. Kushwaha, J. Krizan, T. Liang, R. J. Cava, and N. P. Ong, Anomalous conductivity tensor in the Dirac semimetal Na₃Bi, *EPL (Europhysics Letters)* **114**, 27002 (2016).
- [89] N. Ashcroft and N. Mermin, *Solid State Physics* (Cengage Learning, 2011).
- [90] I. Mandal, Linear response of tilted anisotropic two-dimensional Dirac cones, [arXiv e-prints \(2024\)](#), [arXiv:2412.13978 \[cond-mat.mes-hall\]](#).
- [91] D. Xiao, Y. Yao, Z. Fang, and Q. Niu, Berry-phase effect in anomalous thermoelectric transport, *Phys. Rev. Lett.* **97**, 026603 (2006).
- [92] S. L. Adler, Axial-vector vertex in spinor electrodynamics, *Phys. Rev.* **177**, 2426 (1969).
- [93] J. S. Bell and R. Jackiw, A PCAC puzzle: $\pi^0 \rightarrow \gamma\gamma$ in the σ model, *Nuovo Cim. A* **60**, 47 (1969).
- [94] H. Nielsen and M. Ninomiya, The Adler-Bell-Jackiw anomaly and Weyl fermions in a crystal, *Physics Letters B* **130**, 389 (1983).
- [95] P. Hosur and X. Qi, Recent developments in transport phenomena in Weyl semimetals, *Comptes Rendus Physique* **14**, 857 (2013).
- [96] D. T. Son and B. Z. Spivak, Chiral anomaly and classical negative magnetoresistance of Weyl metals, *Phys. Rev. B* **88**, 104412 (2013).
- [97] A. Ahmad and G. Sharma, Chiral anomaly and longitudinal magnetoconductance in pseudospin-1 fermions, [arXiv e-prints \(2024\)](#), [arXiv:2412.10500 \[cond-mat.mes-hall\]](#).
- [98] K. Das and A. Agarwal, Berry curvature induced thermopower in type-I and type-II Weyl semimetals, *Phys. Rev. B* **100**, 085406 (2019).
- [99] I. Mandal and K. Saha, Thermopower in an anisotropic two-dimensional Weyl semimetal, *Phys. Rev. B* **101**, 045101 (2020).
- [100] I. Mandal and S. Gemsheim, Emergence of topological Mott insulators in proximity of quadratic band touching points, *Condensed Matter Phys.* **22**, 13701 (2019).
- [101] I. Mandal and K. Ziegler, Robust quantum transport at particle-hole symmetry, *EPL (EuroPhys. Lett.)* **135**, 17001 (2021).
- [102] R. M. Nandkishore and S. A. Parameswaran, Disorder-driven destruction of a non-Fermi liquid semimetal studied by renormalization group analysis, *Phys. Rev. B* **95**, 205106 (2017).
- [103] I. Mandal and R. M. Nandkishore, Interplay of Coulomb interactions and disorder in three-dimensional quadratic band crossings without time-reversal symmetry and with unequal masses for conduction and valence bands, *Phys. Rev. B* **97**, 125121 (2018).
- [104] I. Mandal, Fate of superconductivity in three-dimensional disordered Luttinger semimetals, *Annals of Phys.* **392**, 179 (2018).